Geophysical and geological analysis of fault activity and seismic history of the Obion River Area, New Madrid Seismic Zone (NMSZ), Western Tennessee, USA

Author: Jake Joseph Martin

Boston College

The Graduate School of Arts and Sciences

Department of Earth and Environmental Sciences

GEOPHYSICAL AND GEOLOGICAL ANALYSIS OF FAULT ACTIVITY AND SEISMIC HISTORY OF THE OBION RIVER AREA, NEW MADRID SEISMIC ZONE (NMSZ), WESTERN TENNESSEE, USA

a thesis by

JAKE MARTIN

submitted in partial fulfillment of the requirements

for the degree of

Master of Science in Geology and Geophysics

December 2014

Abstract

Thesis Title: Geophysical and Geological Analysis of Fault Activity and Seismic History of the Obion River area, New Madrid Seismic Zone (NMSZ), Western Tennessee, USA

Candidate Name: Jake Martin

Thesis Advisor: John Ebel

The New Madrid Seismic Zone (NMSZ) is well known for producing some of the largest intra-cratonic earthquakes within the North American Plate. The common hypothesis for the geological structure within the NMSZ is that stress is released across three major faults: the Cottonwood Grove Fault, the New Madrid North Fault, and the Reelfoot Thrust Fault. Evidence exists that would suggest an alternative model of geologic deformation in the area: that stress is being released across more than these three faults. A geologic and geophysical investigation was done to investigate a hypothetical fault west of Dyersburg, TN to test the alternative multi-fault hypothesis. A seismically created sand blow was logged in close proximity to the fault projection. Weathering of the sand blow indicated that the age of the sand blow came from a seismic event prior to the 1811-1812 earthquakes. There was no evidence to confirm this sand blow was created by a hypothetical fault in close proximity. A seismic exploration of the area was done across four seismic lines, primarily mapping Quaternary-age Mississippi River flood plain deposits. These seismic surveys yielded no evidence to suggest the presence of an additional fault. Across all surveys no evidence was found to conclusively support any existing theory on fault movement in the NMSZ.

Table of Contents

List of Figures

List of Tables

Introduction

The New Madrid Seismic Zone (NMSZ; central United States), known best for three large earthquakes (**M** 7.3-7.8) between December 1811 and February 1812, is an area that has been extensively studied and is well documented as producing some of the largest intraplate earthquakes within the North American Plate (Gomberg and Ellis, 1994; Johnston and Nava, 1995; Tuttle and Schweig, 1995; Liu and Zoback, 1999; Tuttle, 2001; Tuttle et al., 2002). This seismic activity also includes some of the largest documented earthquakes in cratonic North America during the Holocene (Johnston, 1996).

The recent activity of earthquake activity in the NMSZ is related to the re-activation of the Reelfoot rift, a late-Proterozoic/early Paleozoic aulocogen that runs through the center of the NMSZ (Figure 2). Formation of the Reelfoot Rift was the result of continental rifting and movement along basement faults in Precambrian crystalline rock. The Reelfoot rift is concentrated at zones of structural weakness and serves as the foundation for faulting in the NMSZ (Figure 3; Csontos et al., 2008). Intense shaking related to earthquakes along these faults has formed large fields of sand blows (~10,000 km^2) in this region (Figure 1, Tuttle et al., 2002).

The common hypothesis to explain which geologic structures are associated with the seismic activity in this area is that deformation due to the release of intraplate tectonic stress is distributed over three main faults: the New Madrid North Fault, the Cottonwood Grove Fault, and the Reelfoot Fault (Figure 2, Van Arsdale et al., 2000; Van Arsdale and TenBrink, 2000; Mueller and Pujol, 2001). An alternate tectonic model for the NMSZ is that there is a deep-seated fault at about 15 km depth called the New Madrid Fault, above which several left-stepping en echelon fault segments branch out in the brittle upper crust (Figure 4,

Tavakoli et al., 2010). This latter model is based on high-resolution earthquake data with repositioned earthquakes, revealing segments of the New Madrid North Fault and Cottonwood Grove Fault not initially detected by focal mechanism analysis (Dunn et al., 2010). Structurally, in this model these faults form a flower structure of multiple parallel fault branches (Figures 4-5; Tavakoli et al., 2010) rather than the z-shape of active faults associated with the three-fault model (Figures 2-3).

Independent evidence has been found to support the model that deformation in the NMSZ is distributed over more than three faults. Focal mechanism studies of earthquakes in the area indicate the possibility of an alternate geometry of the three faults; the alignment of these focal mechanisms indicates faulting farther to the northeast than previously believed (Shumway, 2008). The linear projection of strikes of sand dikes exposed in the Wolf River and subsurface altered paleochannels observed in seismic reflection surveys east of Memphis, TN revealed two Quaternary-age faults that are not part of the Cottonwood Grove, New Madrid North, and Reelfoot faults (Figure 6; Velasco et al., 2005). A separate seismic reflection survey in the Kentucky bend area of the NMSZ revealed complex neotectonic features resembling flower structures that were observed in multiple seismic sections, suggesting a different model of regional faulting than currently is thought to exist (Figure 7; Woolery et al., 1999).

Supporting the fault model proposed by Tavakoli et al. (2010) of multiple parallel faults within the NMSZ are observations made by Dr. Martitia Tuttle in autumn 2000, who found a sand dike and sand blow southwest of Dyersburg, TN in the cutbank of the Obion River at field site OR216 (Figure 8, Tuttle and Schweig, 2001). The 1.6 m wide sand dike strikes N35°E-N46°E, and the overlying sand blow is reworked and buried by 1 m of fluvial

deposits. The soil horizon beneath the sand blow is displaced vertically across the dike by at least 1 meter in such a way as to suggest that it was caused by faulting and not by deformation associated with the sand blow. Radiocarbon dating of *in situ* tree trunks provided an age proximal to the New Madrid earthquake sequence of 1450 C.E. ± 150 yr. While the depth to the base of the liquefied unit was not measured, previous borehole studies of similar sand blows in this locality have recorded depths to the base at 25 m (Tuttle and Barstow, 1996).

At roughly the same strike as the sand dike are sand fissures observable in black and white aerial photography; each set of sand fissures trend three kilometers to the north-northeast of OR216 and project to intersect with the sand dike (Figure 9; Tuttle and Schweig, 2001). The strike of these sand fissures also run near-parallel to the strike of the New Madrid North and Cottonwood Grove strike-slip faults, indicating that these sand fissures are fault lineaments. The presence of these lineaments raises the question of whether the feature seen at OR216 is an isolated local feature or whether it is part of a larger fault branch that has had significant fault displacement in past large earthquakes. The discovery of a fault striking near-parallel to the Cottonwood Grove and New Madrid North faults would support the idea that deformation in the NMSZ does not occur over a single set of faults, but rather along multiple, parallel strike-slip faults (Tavakoli et al., 2010).

In this thesis, I present the results of three seismic reflection survey lines collected in August 2010 outside of Dyersburg, TN and of a separate fourth seismic line collected by students of Dr. Lorraine Wolf in 2003 (Figure 10). These seismic lines were run within 0.5 kilometers of OR216 and intersected the projection of the hypothesized strike-slip fault at approximately a perpendicular angle. The goal of this research was to seek any evidence of

subsurface displacement along the strike of the projection of the hypothesized fault inferred at OR216 that could be correlated to fault movement.

Geologic Background

Faulting Behavior

There have been several geological and geophysical studies that have tried to image and interpret the three major identified faults (Figure 1,2) in the New Madrid region (USGS, 2011). The Reelfoot Fault, a northwest-trending reverse fault, has been imaged by reflection profiles crossing the fault; from these profiles a total displacement of 5.4 m, at a displacement rate of about 6.2 mm/year, has been calculated from 900 C.E to 1812 C.E. (Figure 11; Van Arsdale, 2000). Faulting occurs 5 km to 15 km deep and dips along planes at 32° to 55° (Csontos and Van Arsdale, 2008). The configuration of the Cottonwood Grove Fault was established by focal mechanism studies of five $M \geq 4.0$ earthquakes as a northeast-trending right-lateral strike-slip fault that trends approximately along the Missouri-Arkansas border, with the fault striking N40ºE (Herrmann and Canas, 1978). The Cottonwood Grove Fault extends 150 km northeast from Ridgely, Tennessee, terminating at the Reelfoot fault (Mueller and Pujol, 2001). The New Madrid North Fault, the northern branch of the active seismic zone, has an estimated recent displacement of at least 13 meters based on the displacement of a Holocene paleochannel (Guccione et al., 2005). Seismic reflection profiles of the New Madrid North Fault have recorded displacement along the fault to observed depths of 70 meters, with faulting extending into basement rock (Figure 12; Baldwin et al., 2005). The combination of rupturing along these three faults has been determined as the origin of the earthquake activity during the 1811-1812 earthquakes (Mueller et al., 2004).

Lithology

There are six major near-surface sedimentary geologic units in the portion of the New Madrid Seismic Zone where the Mississippi Embayment is found, based on well log, seismic reflection, and outcrop data collected in the region, including my study area OR216 (Van Arsdale and TenBrink, 2000). Using the Van Arsdale and TenBrink (2000) seismic and well log survey information, including subsurface contour maps they constructed, I was able to identify the unit thicknesses in my study area. I also found that the unit thicknesses to be within 10 meters of those from Reelfoot Lake, TN, with extensive documentation of the Reelfoot Lake stratigraphy from geological and seismic reflection surveys in Van Arsdale and TenBrink (2000) and Cox and Van Arsdale (2002) (Figure 13).

The topmost unit in my study area is composed of Quaternary-age modern fluvial deposits related to the movement and evolution of the Mississippi River (Cox and Van Arsdale, 2002). This includes all of the typical deposits seen with a meandering river system: predominantly clay-sized floodplain deposits and sand-sized channel deposits, including iron and calcite nodules that alternate stratigraphically as a result of channel migration (Aslan and Autin, 1998). The thickness of the Mississippi flood plain deposits varies depending on location, but at Reelfoot Lake they been measured at 135 feet (45 meters) (Saucier, 1994).

Below the Holocene fluvial deposits lies the Jackson formation, a late-Eocene-age fluvial/deltaic silty sand interbedded with lignite and clayey silt. The thickness of the unit is variable within the NMSZ; the Mississippi River has eroded portions of it. However, the thickness of the Jackson in my study area is estimated to be 135 feet (45 meters) (Austin et al., 1991). Underlying this is the Eocene-age Claiborne Group, comprised of the Cockfield Formation, the Cook Mountain Formation, and the Memphis Sand. These units transition

top-down from clayey silts interbedded with sand and lignite downward to a fine-to-coarse grained sand, with the entire group interpreted to be a transgressive ocean sequence (Van Arsdale and TenBrink, 2000). The total thickness of the Claiborne Group is estimated as 778 ft (260 m): the Cockfield Formation is estimated as 145 ft (46 m) thick, the Cook Mountain Formation is 178 ft (60 m) thick, and the Memphis Sand is estimated as 455 ft (150 m) thick (Van Arsdale et al., 1998).

The next set of formations below the Claiborne group comprise the upper-Paleocene Wilcox group, which includes the Flour Island Formation, a fluvial/deltaic sand 138 ft (45 m) thick; the Fort Pillow Sand, a marine sand about 153 ft (50 m) thick; and the Old Breastworks Formation, a clayey silt sand about 387 ft (130 m) thick (Van Arsdale and Tenbrick, 2000). Beneath these units is the Porters Chalk Clay, a lower-Paleocene marine clay about 314 ft (105 m) thick). There is then a large gap in time locally, with the Porters Chalk Clay lying unconformably on the McNairy Sand, a calcareous fine-grained to coarse-grained marine sand unit estimated as 317 ft (~105 m) thick. Underneath this is Paleozoic-aged dolomite, the effective bedrock in the New Madrid Seismic Zone region (Van Arsdale et al., 1998).

Regional Liquefaction

Earthquake-induced liquefaction is a major near-surface geomorphic process in this region; a large liquefaction field (~10,000 km^2) has been attributed to the NMSZ (Tuttle et al., 2002). Seismic liquefaction is the change of sediment from a solid state into a liquid-like state as the result of rapidly increasing pore-water pressure caused by intense shaking from earthquake activity. When a water-saturated sand unit that is confined by a fine-grained surficial layer is shaken by an earthquake, the shear stress causes a buildup of pore-water

pressure in the saturated sand and can result in liquefaction, eventually inducing venting upward of the sand unit through the fine-grained surficial layer. These types of features are particularly abundant in the NMSZ due to the combination of fluvial deposits, high-intensity past earthquake activity, and a lack of local erosional processes across the entirety of the NMSZ that would remove evidence of liquefaction (McCalpin, 1996).

A most pronounced surface feature of liquefaction generated by earthquake shaking is the sediment that has vented to the ground surface, which produces a fining-upward sequence of laminated sand known as a sand blow. In sand blow lithology the surface unit is fed by a linear sand dike running vertically or near-vertically and cutting through the fine-grained surficial layer that existed prior to the earthquake. The bedding of the underlying sand unit is disrupted by the venting of sand at the point where the fine-grained surficial layer is ruptured. The depth of the source sand unit feeding the sand dikes and sand blows can be as deep as 25 meters in the NMSZ region (Tuttle, 2001).

The combination of a circular sand blow with a corresponding feeder dike indicates that liquefaction occurred due to shaking generated by an earthquake (McCalpin, 1996). The earliest documented studies of liquefaction features in the NMSZ reported dome-like accumulations of unweathered, well-sorted sand deposits on the ground surface that are attributed to the 1811-1812 earthquakes (Fuller, 1912). These circular sand blow deposits were observed in early studies to reach thicknesses greater than 1 m and to have a diameter of up to hundreds of meters within the NMSZ around the Missouri-Tennessee border (Fuller, 1912). Later studies of liquefaction in the NMSZ determined three major influences on the sizes of sand blows within the NMSZ: 1) the liquefaction susceptibility of sediment

(influenced by grain size); 2) the thickness of the overlying capping layer; and 3) the proximity of an earthquake's focus to the site (Obermeier, 1989).

Radiocarbon dating of sand blows throughout the NMSZ has established evidence of 1450 C.E. and 900 C.E. earthquake events in addition to the 1811-1812 earthquakes (Tuttle et al., 2002). Using the current fault model of the NMSZ (Figure 1), an empirical relation between earthquake moment magnitude and the distance to the farthest sand blows dated to the 1811-1812 events yield a magnitude of 7.6 for at least one of the 1811-1812 earthquake events (Tuttle et al., 2002). More recent studies have put magnitude thresholds of 6.7-7.9 for the December 1811 event, 6.9-7.8 for the January 1812 event, and 7.0-8.1 for the February 1812 event (USGS, 2011). Although not all of the known sand blows have been documented and dated around Dyersburg, the stratigraphy, thickness, and spatial distribution of known sand blows of common radiocarbon ages could be used to determine the magnitude of an earthquake on the postulated OR216 fault (Figure 14; Tuttle et al. 2002).

Weathering characteristics of sand blows in the NMSZ have also been used to estimate ages of sand blows and to correlate those sand blows to previous seismic events in the area (Tuttle et al., 2005). Degree of weathering can be correlated to age of the sand blow because soil amounts and properties develop systematically with age, with the rate of formation being a function of the local environment (Harden and Taylor, 1983). One of the main ways weathering can be evaluated is by soil chroma, or "purity of color", by the Munsell color system, which is the color system used to identify colors of soils. In the case of the NMSZ, surficial sand blows that formed during the 1811-1812 earthquake events have minimal soil formation, primarily consisting of Entisols with a chroma of 0-2 on the Munsell

color system; older earthquake events have more extensive and developed soils, primarily Inceptisols with a chroma of 4 or greater and are darker in hue compared to Entisols (Tuttle et al., 2000; Soil Survey Staff, 2010).

In addition to age, sand blows can be used to constrain certain characteristics of historic earthquakes. There are two primary correlations of sand blow characteristics that can be used to constrain the characteristics of an earthquake event. The first relationship is that the magnitude of an earthquake is proportional to the maximum distance between the earthquake epicenter and the sand blow; the second relationship is that a sand blow's diameter is inversely proportional to the distance between earthquake epicenter and the sand blow (Figure 15). Since both the magnitude of the earthquake and the diameter of the sand blow can be related to the distance between the sand blow and the epicenter of the earthquake, it is possible to constrain the magnitude of an earthquake using the diameter of the sand blow (Castilla and Audemard, 2007).

Study Methodology, Results, and Analysis

Sand Blow Investigation

In August 2009, I examined several sand blows with M. Tuttle in Lenox, TN northwest of OR216 and in the vicinity of the projection of the potential fault indicated by the sand fissure lineaments (Figure 10). I measured one sand blow that was found along Lenox Road of Lenox, TN. This feature was selected for logging because the degree of weathering of the sand blow indicated that the sand blow formed prior to the 1811-1812 earthquakes. If a fault is confirmed at OR216 and if the sandblow was formed due to an earthquake on this fault, the diameter of the sand blow could be used to constrain the magnitude of that earthquake.

At the time of my investigation, a long ditch had been recently excavated by the US Army Corps of Engineers along the side of Lenox Road in Lenox, TN, exposing portions of a sand blow that was previously covered by younger materials, but which was exposed as of August 2010. During the summer of 2009 I worked with Natasha McCallister, Michael Towle, and Dr. Martitia Tuttle to excavate, clean, and log the sand blow observed in that ditch in order to better measure the size of such features in this area. The entire sand blow covered 50 meters from end to end and at its thickest had 1 m of erupted sand.

There were five sand units observed in the sand blow section (Figure 16), with three sand units stacked upon each other in some portions of the sand blow, possibly indicating multiple earthquake events. The sand comprising the sand units coarsened at depth and transitioned from lighter to dark shades of yellow and brown at depth. Three individual sand dikes were also observed to intersect with the sand blows and extend at depth below the excavated portions of the section; unfortunately, the trench was not dug deep enough to find the source layer of the sand blow. The sand blows were covered by a layer of alluvium; the alluvium was covered by a layer of "ditch spoil" from the ditch when it was dug.

Radiocarbon dating is the best method for providing an age constraint for the timing of liquefaction; however, no samples adequate for carbon dating were found on site during the investigation of this sand blow. Because of this, while the age of the liquefaction feature at OR216 is known through radiocarbon dating to be ~1450 C.E., the approximate age of the sand blow logged on Lenox Road can only be constrained based on the sand blow weathering characteristics and on its setting within the local stratigraphy. Observing the sand blow logged on Lenox Road, I found the color of the sand to correlate with a larger chroma value, or the saturation of color of a soil; a larger chroma value would correlate the

soil type of the sand blow to an Inceptisol. The chroma value of the sand blow suggests that the sand blow was formed by an earthquake event that predates the 1811-1812 earthquakes, with the age more in line with the 1450 C.E. NMSZ seismic event that created the sand blow at OR216.

Given the proximity of the sand blow to both the hypothetical fault at OR216 and the three known faults in the NMSZ, it is impossible to determine the origin of the seismic event that formed the sand blow based on distance alone**.** There is also no meaningful difference in the distance from the closest projection point of the hypothetical OR216 fault to the Lenox Road sand blow (Figure 10), regardless of whether the source of the seismic energy that created the sand blow is a strike-slip fault (such as hypothesized at OR216) or a thrust fault (such as the Reelfoot Fault) (Castilla and Audemard, 2007).

The possible magnitude of the earthquake that generated the seismic energy required to create the Lenox Road Sand Blow can indicate the seismic source that formed the Lenox Road sand blow itself. Following Castilla and Audemard (2007; Figure 15), the lowest earthquake magnitude observed to generate a sand blow from a strike-slip fault of the sand blow diameter seen at Lenox Road is **M** 5.5 (Castilla and Audemard, 2007). In order for a strike-slip fault to create an **M** 5.5 earthquake the length of the rupture would need to be at minimum 3.3 km (Wells and Coppersmith, 1994). Using the length of the sand fissures observed intersecting OR216 to approximate the length of the hypothesized fault at OR216, the current projected length of the fault would be less than the length necessary to create an M 5.5 earthquake by 0.5 km. In contrast, the estimated magnitude of the 1450 earthquake event from the larger NMSZ earthquakes is sufficiently large enough to generate the sand

blow observed along Lenox Road, making it highly probable that the Lenox Road sand blow was generated by one of the known active faults in the NMSZ.

Seismic Reflection Survey

Three shallow seismic-reflection lines were acquired west of Dyersburg, TN within 0.5 km of the OR216 liquefaction site during summer 2010: Line W, Lines V and V_A, and Lines R and R_A (Figure 10). Given the proximity of certain parts of seismic lines, I have chosen to present them as a single line. The purpose of my 2010 survey was to acquire a seismic reflection image as close as possible to OR216 with a seismic line that perpendicularly intersected the possible fault lineaments. If there is a fault at OR216, by extension that would support the hypothesis that there are multiple, parallel active faults in the NMSZ region, and those faults could form the flower structure proposed by Tavakoli et al. (2010) (Figure 5). In a seismic profile, the best chance of observing evidence of faulting would be to observe the vertical displacement of horizontal units that have been offset by the faulting, since seismic surveys are unable to image vertical faults directly (Figure 17). Seismic reflection also is capable of generating high-resolution images at depths greater than 25 meters; since the maximum depth of liquefaction observed in the NMSZ is 25 meters, any observed subsurface displacement observed at depths greater than 25 meters could be assumed to be due to faulting and not have been caused by liquefaction.

Seismic surveys were chosen to try to detect the suspected fault because they provide higher-resolution imagery at depth compared to other geophysical techniques available at the time of the survey, including ground-penetrating radar. The seismic lines I collected in 2010 were acquired using an RAS-24 Seistronix seismograph utilizing a single-end spread source/geophone configuration and a sledgehammer/plate seismic source. The receiver

spread consisted of 24 geophones with spacing of 0.5 m or 1 m, depending on the amount of space available to collect the seismic lines (Table 1). The source in my seismic survey moved with every shot gather while my geophones were stationary. In addition to the data that I collected, a fourth shallow seismic-reflection line was collected by Dr Lorraine Wolf and students from Auburn University at the same location as line V. The Wolf line used a hammer/plate seismic source spaced 10-12 meters from the first geophone. The Wolf seismic line transitioned from a 24 geophone single-end configuration for the first 86 shots collected to a 48 geophone split-end configuration for the last 28 shots (Table 1).

All seismic reflection data in this thesis were processed using WinSeis Turbo from the Kansas Geological Survey and was processed followed identical steps (Table 2). Parameters used in the data processing steps can be found in the appendix. While the process for the steps within seismic processing can be somewhat fluid, all the steps applied during this process can be characterized as "standard" unless otherwise noted (such as for poor data quality).

Step 1: Data were converted to the KSG format used by WinSeis Turbo.

Step 2: Traces that were observed as being dead or significantly higher amplitude due to problems with the field recording were killed, or muted entirely, using WinSeis (Figure 18). Issues with the data quality of the traces that required killing were linked to poor coupling of some geophones with the ground that gave excessive noise and to mechanical issues with some geophones that resulted in dead traces.

Step 3: A surficial mute of first-arrival P-waves was carried out using WinSeis. While useful for seismic refraction, the first arrival energy causes artifacts in reflection profiles (Figure 19; Steeples and Miller, 1998). I did a first arrival mute of shot-gather data; mutes

typically extended to 10-20 ms based on when the direct wave arrived in the shot-gathered seismic section (Table 1).

Step 4: A band-pass filter was applied to further filter out surface waves in the collected sample. The goal of the band-pass filter is to preserve the maximum amount of body-wave energy while minimizing the effect any surface or air-wave energy that may be obscuring potential reflectors (Figure 19). Surface waves created by the sledgehammer source have lower frequencies (<20 Hz) compared to the body waves being reflected at depth (Claerbout, 1985). The lower frequency cutoff of the band-pass filter will eliminate most of the energy of the surface waves while preserving most of the body wave energy. Conversely, air waves tend to dominate at frequencies of 150 Hz or higher, so the higher frequency cutoff of the band-pass filter will eliminate most the air wave energy (Steeples and Miller, 1998). I used 150 Hz for the high-cut corner of the band-pass filter. To determine the low-cut corner, I measured the periods of potential reflectors in my seismic section. I calculated the frequency of the low-cut corner of the band-pass filter by measuring the period of potential reflectors in my seismic section and inverting the periods to obtain an estimate of the frequency of the reflectors, recording values of 120-150 Hz. In order to filter out surface and air waves while preserving the body waves, I set the value of the low-cut corner of the filter lower relative to the measured frequency of the reflectors, resulting in low-cut corner values ranging from 70-100 Hz.

Step 5: An F-K filter was applied to remove the effects of dominant surface waves and air waves. F-K filters are designed to let energy pass within certain apparent velocities defined by the user. Surface waves and air waves recorded in the seismic section obscure potential reflectors in seismic sections (Figure 20). Surface waves and air waves also have

slower apparent velocities than that of P-wave energy from primary reflections, resulting in steeper slopes for surface and air waves in T-X plots compared to the slopes of primary reflectors (Figure 21). I selected the boundaries for the pie-slice F-K filter by measuring the slopes of reflectors and other waveforms in T-X space and choosing slope values for the filter cutoffs that would include reflectors but exclude as much surface and air-wave energy as possible. Minimum slopes for the F-K filter were 0 ms/trace for all shot gathers, while maximum slopes for ranged from 0.3 ms/trace to 0.6 ms/trace (Table 2; Park et al., 2002).

One consequence of applying the F-K filter to my data was the discovery of a programming error in the WinSeis code that was subsequently confirmed by KSG. This error occurs when F-K filtering and frequency filtering are applied to the same seismic section through the WinSeis program. The result of this error is negative moveout in the first 2-4 traces and no moveout in the last 2-4 traces of the shot-gathered seismic section, which was compensated by the muting of shot-gathers in step 6 (Figure 22).

Step 6: A surgical mute of shot gathers was done to reduce noise in the final CDP-stacked seismic section. I analyzed every shot-gathered section to see if there was negative moveout in any of the first four traces and no moveout in the last four traces of the section. Any traces with these moveout scenarios were determined to have been affected by the F-K programming error detailed in step 5 and therefore were muted (Figure 22).

Step 7: Traces were resorted. With the RAS-24, the traces were automatically sorted to reflect the field geometry of my lines as single-end shot gathers. In this data processing step, I changed the configuration of data from single-end shot gathers (or single-end/split end in the case of the Wolf seismic line) to common midpoints (CMPs) gathers.

Step 8: Kill traces in the CDP-gathered section (not applied to the Wolf seismic line data) to reduce shingling in the stacked seismic section. After performing a brute stack of the seismic section, the section was exhibiting shingling. Shingling is a processing artifact caused by improper muting of first arrival energy that results in the offset of reflectors in seismic sections to the point where reflectors disappear and reappear (Figure 23; Steeples and Miller, 1998. Since muting the first arrivals was not effective in eliminating shingling in my seismic section, I muted entire traces in order to minimize the shingling in my stacked seismic section. I experimented with killing different traces in the CDP-gathered seismic sections (Figure 24) and observed the amount of shingling in each brute-stacked seismic section. Traces were killed in the CDP-gathered section that eliminated the largest amount of shingling in the brute-stacked seismic section (Figure 25).

Step 9: Traces were corrected using a Normal Moveout Velocity of ~1000 m/s applied to the whole section. I applied a range of NMO velocities (400-2000 m/s) to my stacked seismic sections (Figure 26). Through the trial and error of applying NMO velocities, I chose to use an NMO correction of 1000-1200 m/s. Flood plain stratigraphy, such as that in my survey area, produces near-horizontal sub-surface layers, more so for the stratigraphic layers that are closer to the surface (Walker and James, 1992). Since reflectors were not near-horizontal in stacked seismic sections with NMO corrections less than 1000 m/s, I did not choose to use those velocities for NMO correction. Alternately, at higher velocities, static corrections may dominate the periods of the reflection waveforms, particularly with shallow reflectors (Steeples and Miller, 1998). As a result, there may be breaks in reflectors that could be interpreted as faults but are in fact the product of incorrect stacking velocities (Figure 27). These breaks occurred in my stacked seismic section when NMO corrections

greater than 1200 m/s were applied, so I chose not to apply velocities of greater than 1200 m/s to my seismic sections.

Step 10: Automatic gain control was applied to all traces, increasing the amplitude of late-arriving traces to match early-arriving traces.

Step 11: Traces were stacked and then used to create seismic sections for each survey location.

Geophysical Interpretation

The criteria for identification of a potential fault was a) identifying offsets in reflectors and b) identifying such offsets of reflectors continuously downward beyond 25 meters depth. Any previously mentioned features known to be the result of processing errors, such as the F-K programming error (mentioned in processing step 5) and reflector shingling (mentioned in processing step 8) were excluded (Figure 22,25). I treated the NMO correction velocity (~1000 m/s, or 1 m/ms) as the velocity of the underlying material, so the travel time in milliseconds is approximately equivalent to half the depth of a reflector in meters (i.e. 50 milliseconds of two-way travel time equals 25 meters depth). All geologic layer boundaries are extrapolated from Van Arsdale and Cox (2002).

In each subsection below I analyze and interpret the four seismic lines collected in the OR216 study area. This includes identification of reflectors in each seismic section, correlations of reflectors between sections, geologic/geomorphic interpretation, and potential subsurface displacement. The goal is to properly contextualize each seismic section in order to identify subsurface displacement that could be related to faulting.

Detailed seismic line configurations can be found in the appendix.

Woods Seismic Line

The woods seismic line (W Line) was taken 10 meters from OR216 in a heavily forested area. Four distinct reflectors were observed in the final processed seismic section, with a fifth, truncated reflector seen at 30 m depth (Figure 29). There are also two weak reflectors observed at depths of 5 m and 10-12.5 m. It is highly probable that the 5 m reflector correlates to an abandoned river channel observed at the site, as the reflector dips towards the abandoned channel. Based on previous geological surveys of the region (see "Lithology" section of thesis), the entire seismic section falls within Quaternary-age Mississippi Flood Plain deposits. The projected unit boundary for these units is ~45 meter deep; the depth of my seismic section was limited to ~40 meters, as indicated in Figure 29. There is no evidence of subsurface fault displacement in the section; all reflectors are continuous and have no apparent breaks that could be correlated to fault displacement.

V and V_A Seismic Lines

The Vestal farm lines (V and V_A) were taken along a dirt road to a farmhouse owned by Tim Vestal. The line was split into two portions because the road changed direction towards the southeast by 10-15 degrees, but the lines are still consecutive. In line V there is only one coherent reflector across the entire profile, seen at ~10-15 m depth, with partial reflectors at depths of 17.5 and 25 meters (Figure 30). Two of the three reflectors (at 10 and 17.5 m) are also seen in V_A; there is also some residual energy visible at 25 m, but it does not form a clear reflector when processed (Figure 31).

As with line W, the entirety of the seismic section falls within Mississippi flood plain deposits identified by Van Arsdale and TenBrink (2000). The depth of the boundary between the Jackson Formation and Mississippi flood plain is 45 m, while the greatest depth

at which I observed coherent reflectors was ~35 m. There is some displacement in the three reflectors at CDP 105 (Figure 30). However, I have attributed that displacement to shingling rather than to the presence of a fault because of the amplitude change seen in the reflectors, an abrupt pattern change that is inconsistent with a diffraction or other indicators of subsurface displacement.

R and R_A Seismic Lines

The road lines (R and R_A) were taken along the side of a paved road outside of the Vestal farm property. The lines are separated by a 10 m long bridge. There are two reflectors seen in Line R at 20-25 m depth and 30-35 m depth that converge at CDP 83, where they merge into a single reflector (Figure 32). There is also a third reflector at 45 m depth that disappears and reappears across the section. All three reflectors seen in section R are also observed in line R_A (Figure 33).

Reflectors at the top of the seismic section appear to dip toward the west, while reflectors at greater depth appear to dip towards the east, although that is hard to resolve due to the amount of shingling seen in the seismic section, particularly at CDPs 73-75. As with lines W, V, and V_A, the entirety of lines R and R_A fall within Mississippi flood plain deposits. There is also a possible diffraction observed at CDP 25-30 22.5 m deep, which is possible evidence of subsurface displacement. Diffractions are the result of abrupt discontinuities in structures; in geology, typical sources of diffractions include faulting, abrupt changes in layer geometry, and isolated objects (such as large rocks) in otherwise homogeneous material (Kearey and Brooks, 1991). While it is possible that the diffraction is the result of faulting, I believe the probability is low that the feature is associated with the

postulated O216 fault given the lack of evidence in other seismic sections for faulting at similar depths.

Wolf Seismic Line

The Wolf Line, collected by Dr. Lorraine Wolf and students from Auburn University, was taken roughly at the same location as the Vestal Farm seismic line. There are three reflectors line at depths of 15, 30 and 45 meters (Figure 34). There are also some processing artifacts seen at CDP 150-180 (as indicated in Figure 34) that are apparently caused by the switch between the single-end and split-end survey. However, there appears to be a diffraction seen at CDP 190-200 at 20 m depth, similar to what was seen in line R, with both diffractions dipping towards the east. That both diffractions were seen at a similar depth and dip in the same direction is evidence that the diffractions are related to each other and may be indicators of subsurface fault displacement.

Discussion

There are three primary conclusions I can draw from the seismic data collected from the OR216 survey area. First, based on depths of geologic units within the Obion River area (as identified by Van Arsdale and TenBrink, 2000), the entirety of the data for all seismic sections collected fall within Quaternary-age Mississippi flood plain deposits. Second, the two reflectors observed ~30 ms and ~40 ms in the majority of seismic sections are most likely lithology changes consistent across all seismic sections; since all units in the section fall within Mississippi Flood Plain, this is probably the result of a flooding event depositing material on existing flood plain deposits. Third, there is no clear evidence of subsurface displacement in the seismic reflection sections. The only possible evidence found for fault displacement would be the diffraction found in Line R (Figure 32). However, the odds

probably are low that this diffraction is the result of subsurface faulting, but more likely it is the result of some other cause that disturbed the subsurface interface in the sediments based on the shallow depth of displacement and absence of evidence in any other seismic section.

Subsurface displacement would be the strongest indicator of faulting in my survey area, but there is no clear evidence of subsurface fault displacement from the seismic surveys collected by myself in 2010 and Dr. Wolf's students in 2003. If there is no evidence for a fault on the projected fault trace that intersects OR216, then the lineaments observed in the aerial photography would have to be explained by another geologic structure. An alternative hypothesis for the cause of the lineaments, given the large number of abandoned river channels in the area, is that the lineaments are filled-in abandoned river channels (Sauicier, 1996).

While there is no conclusive evidence to prove there is a fault intersecting OR216, there is not enough evidence to explicitly disprove the existence of the OR216 fault. Due to limited funding, there was only one week spent collecting data in the OR216 survey area, which only allowed time for the five seismic lines collected. Given more time, a grid coordinate survey within a 1x1 km area of OR216 would have provided a three-dimensional subsurface model for the area. A three-dimensional model would produce a more extensive and comprehensive image of the subsurface stratigraphy, including any possible subsurface displacement of the sedimentary layers (Kearey and Brooks, 1991).

Given no proof of subsurface displacement that can be correlated to faulting, there is no evidence in the seismic surveys I collected to support the model that deformation in the NMSZ is distributed over more than three faults. In addition, while the suggested age of the sand blow observed along Lenox Road correlates to the 1450 C.E. earthquake event and the

age of the sand blow observed at OR216, there was no evidence to definitively suggest the sand blow was created by the result of failure of a fault outside of the New Madrid North fault, Cottonwood Grove fault, and/or the Reelfoot Fault. However, given the lack of conclusive evidence from the seismic surveys, it is difficult for me to definitively prove or disprove the traditional fault model or the multi-fault theory proposed by Tavakoli et al., 2010 based on the survey data I have collected.

Conclusion

In this thesis I have laid out some field investigations in which I tested the commonly accepted hypothesis that within the New Madrid Seismic Zone stress is distributed over three faults. My liquefaction study did yield evidence to support the current NMSZ three-fault theory, but the results of this study were not sufficient satisfaction to reject the multi-fault theory. While I was able to image the subsurface around OR216 and identify the contact between Mississippi fluvial deposits and the Jackson formation, I found no indications of fault displacement at depth in any of my seismic sections. As a result, I have found no conclusive evidence to suggest that such a fault exists at OR216 that would disprove the three-fault theory within the NMSZ.

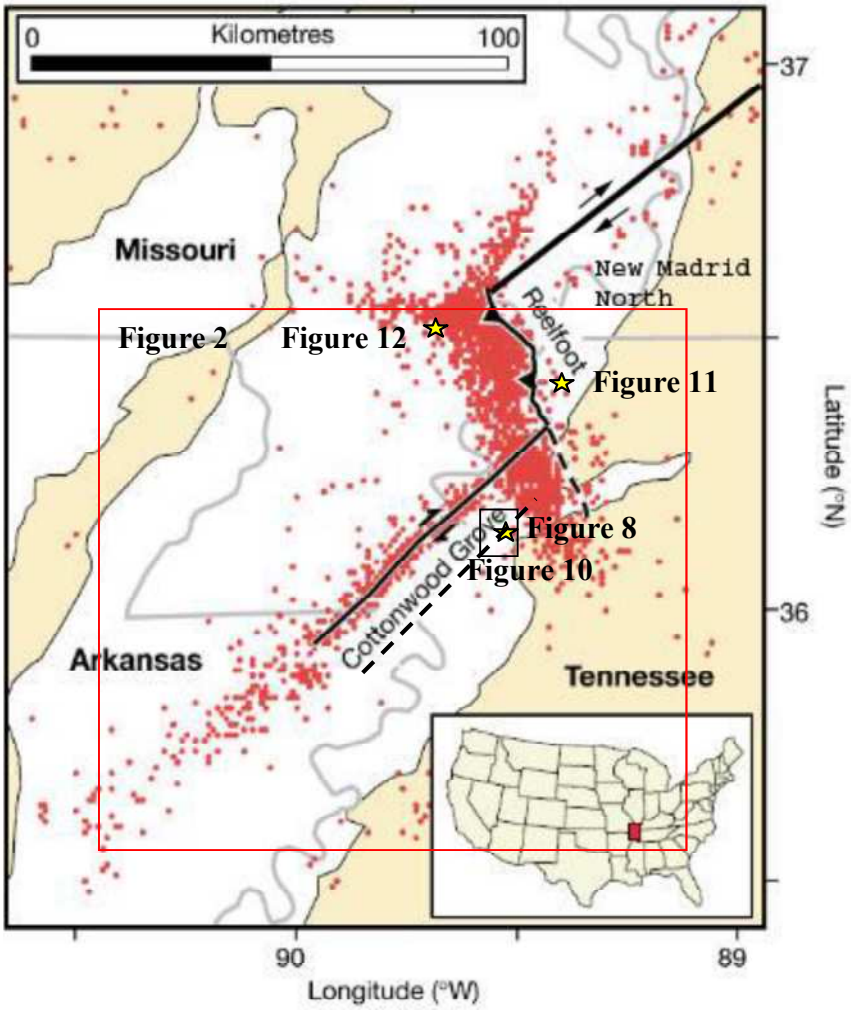

Figure 1: Area of NMSZ with three major faults. The projection of the proposed fault is indicated by dashed line. The area of Figure 2 is indicated by the red box on the map; the area of Figure 10 is indicated by the black box on the map; yellow stars indicates references to other figures (modified from Mueller et al., 2004).

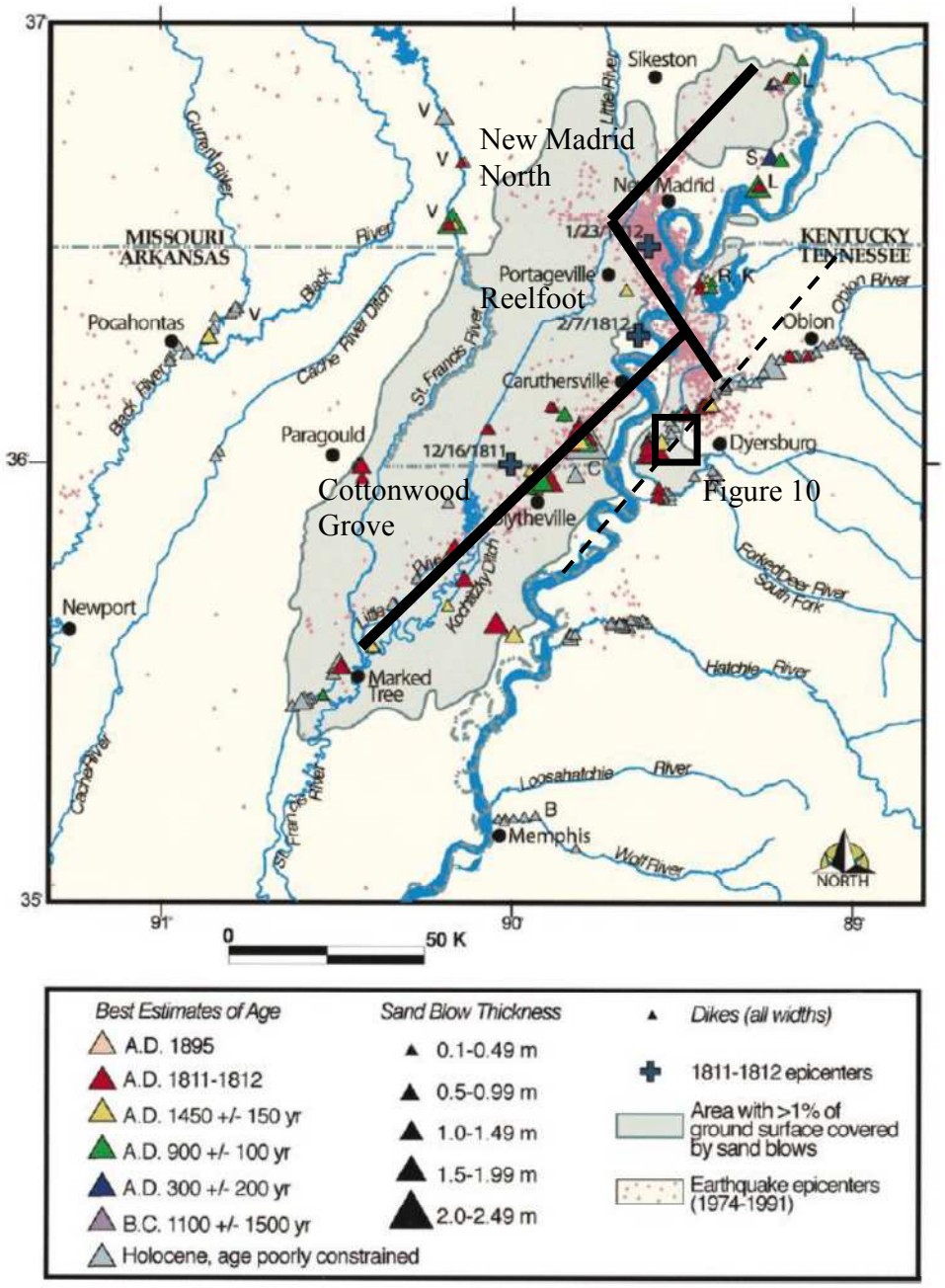

Figure 2: Location of Obion River study area (Figure 10, indicated by black outline), including logged liquefaction features in the area, with faults from Figure 1 projected on map; the projected fault that is sought in this thesis is indicated by the dashed line (modified from Tuttle et al., 2002).

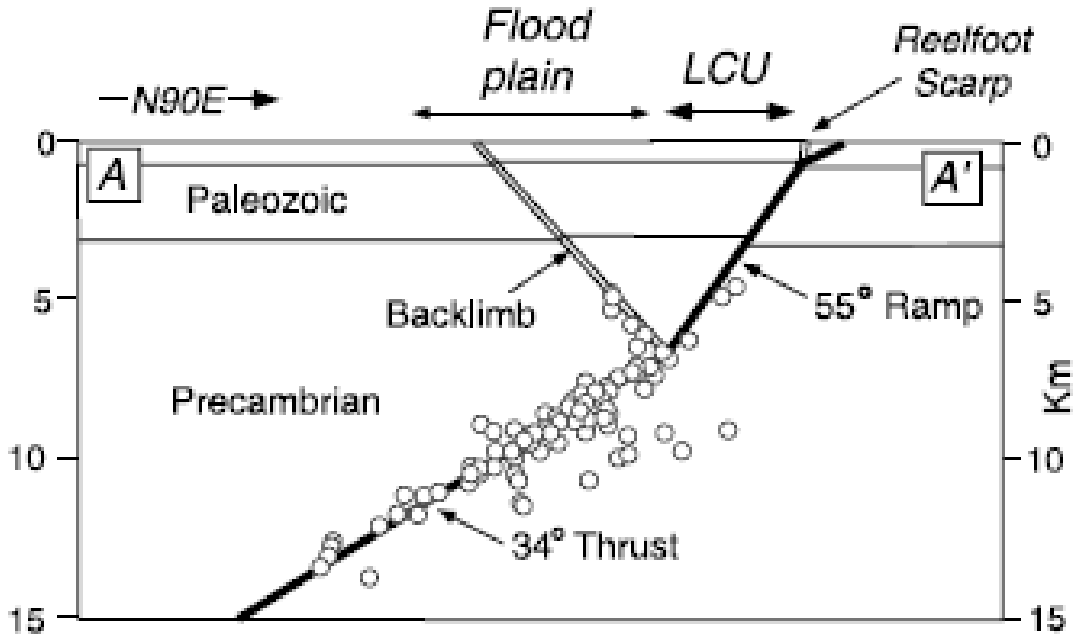

Figure 3: Simplified cross-section of the Reelfoot scarp and the Precambrian-age aulacogen (labeled Thrust) (from Mueller et al., 1999).

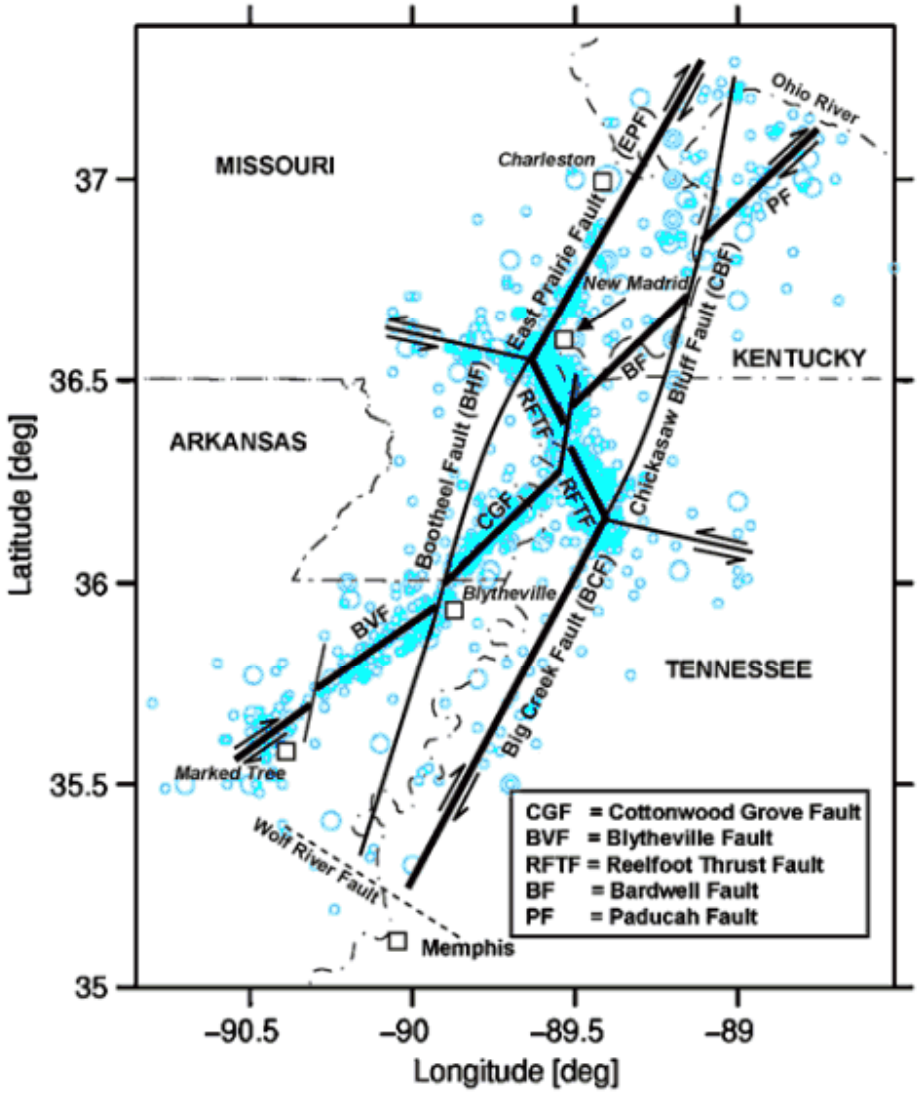

Figure 4: Alternative model for faulting for the NMSZ (modified from Tavakoli et al., 2010).

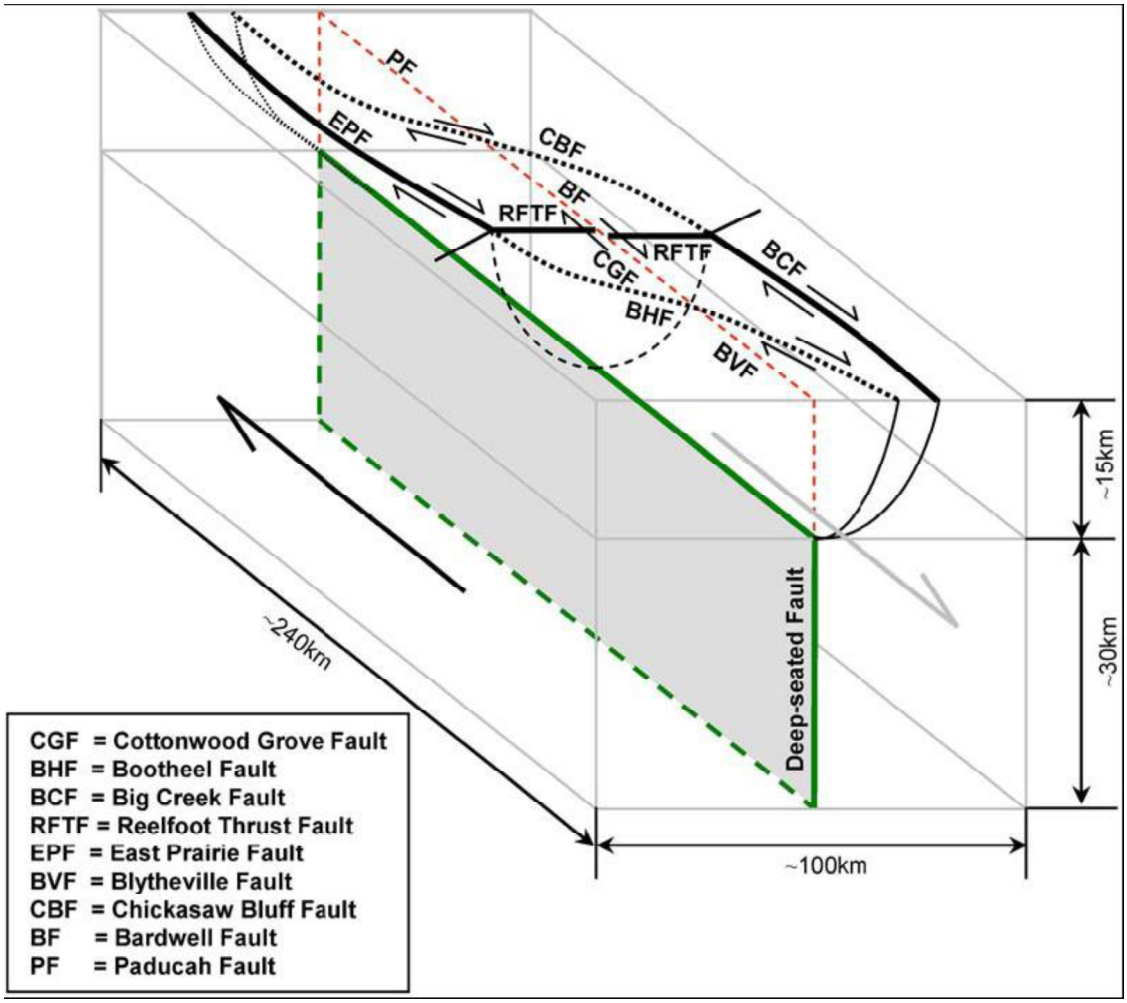

Figure 5: Three-dimensional model of a possible flower structure fault distribution in the NMSZ. Subparallel right-lateral strike-slip faults are concave toward the Reelfoot Rift at depth (modified from Tavakoli et al., 2010).

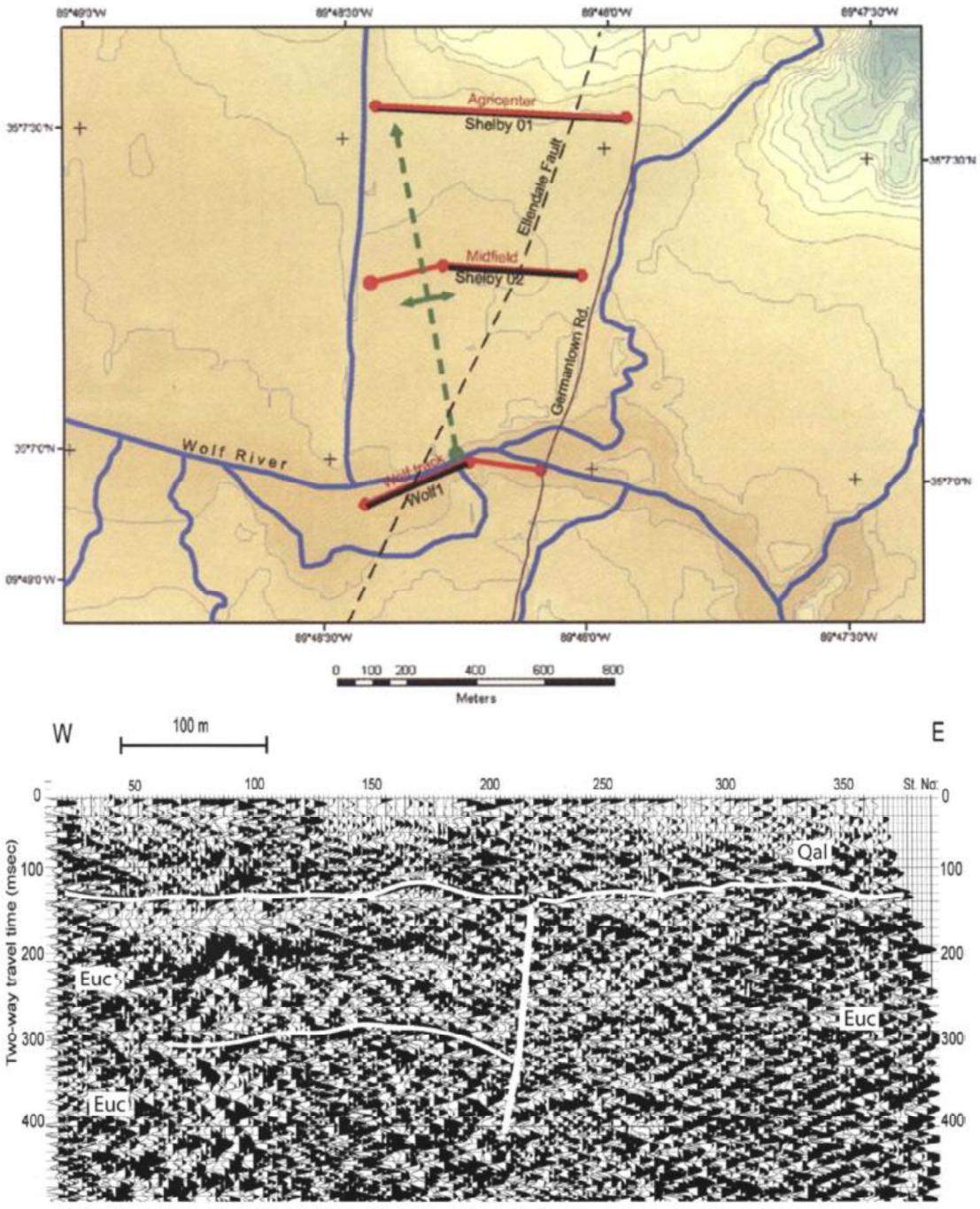

Figure 6: Above: Location of seismic surveys collected around Memphis, TN. Black dashed line indicates one of two faults found in the area, black and red solid lines indicate seismic lines taken, and green lines indicate anticline geometry from the area. Below: Interpreted seismic profile taken from Wolf River near Memphis, TN (Wolf1 seismic line) with inferred displacement due to faulting of upper Claiborne group (Euc) highlighted by vertical white line (from Velasco et al., 2005).

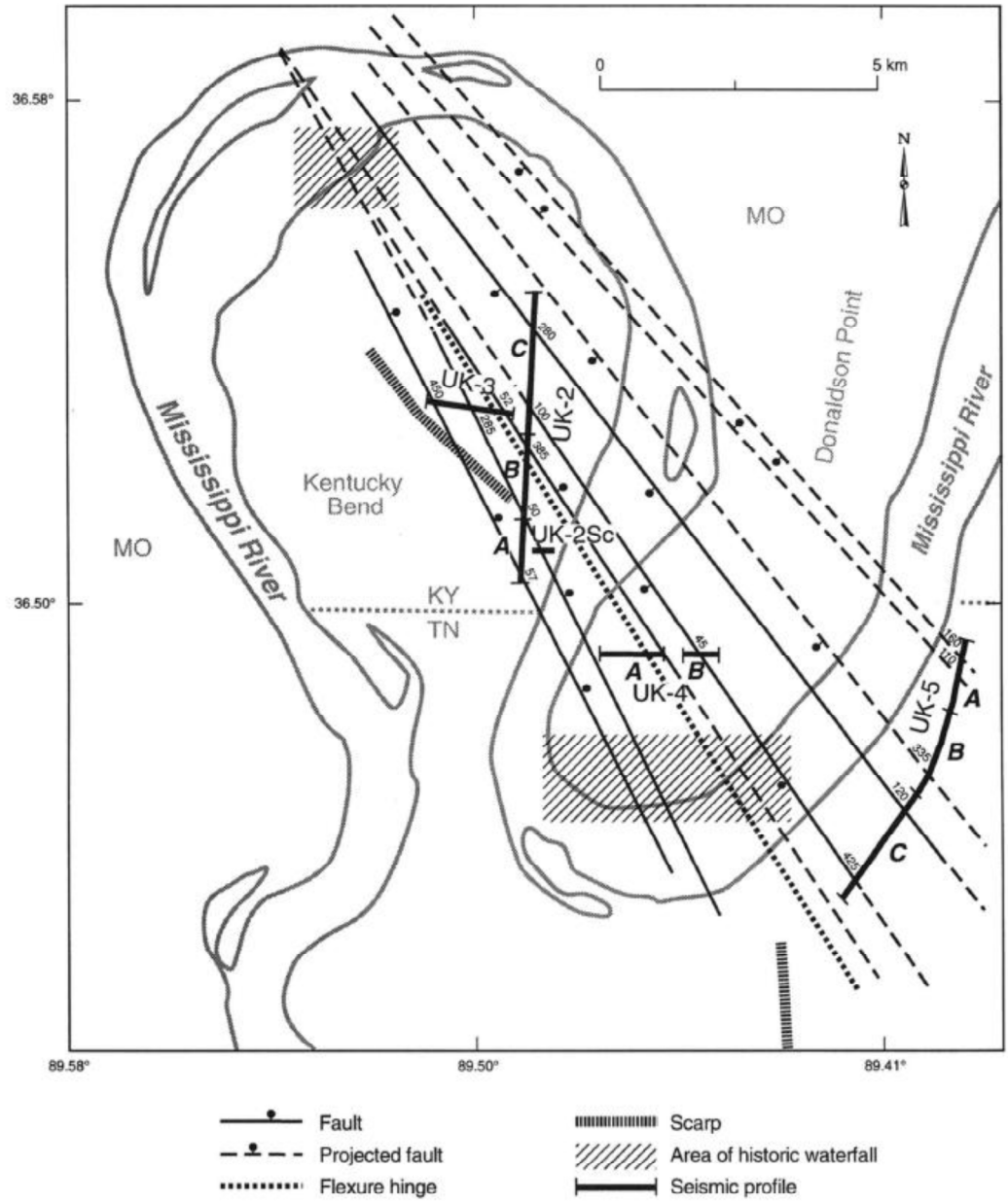

Figure 7: Map of known faults (solid lines) and the projections of faults interpreted from seismic profiles collected east of the NMSZ (dashed lines; from Woolery et al., 1999).

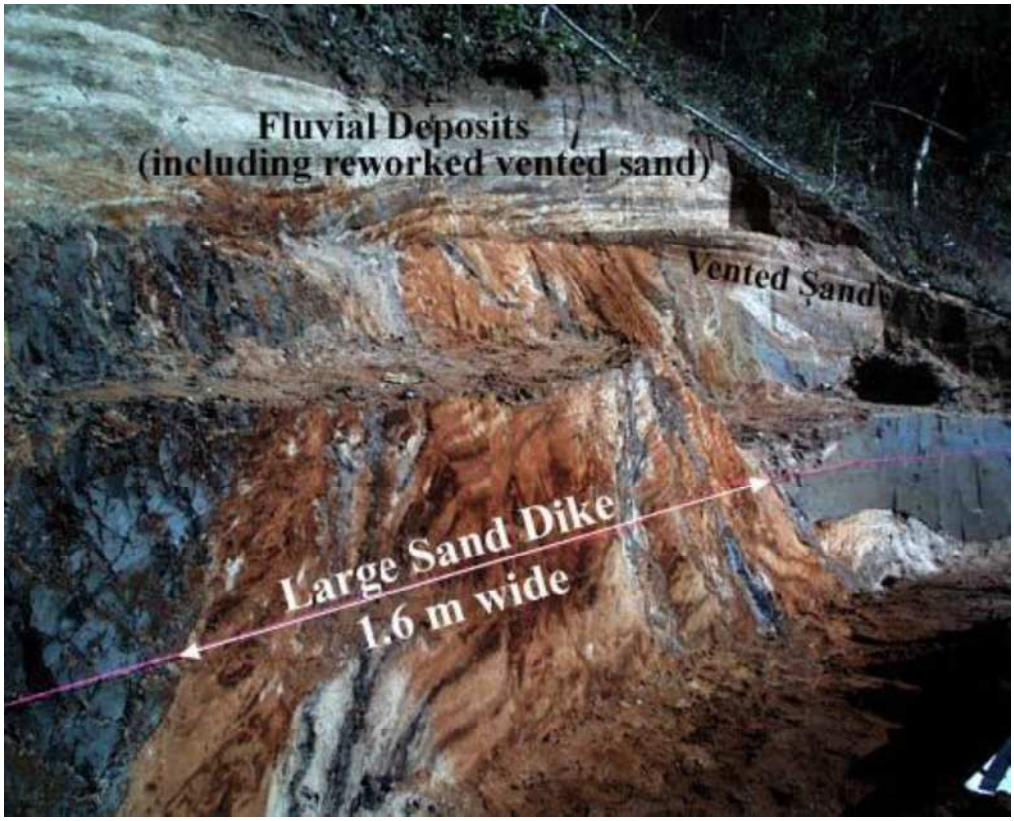

Figure 8: Photograph and log of the liquefaction feature observed at OR216 near Dyersburg, TN, recorded in 2002 (modified from Tuttle and Schweig, 2001).

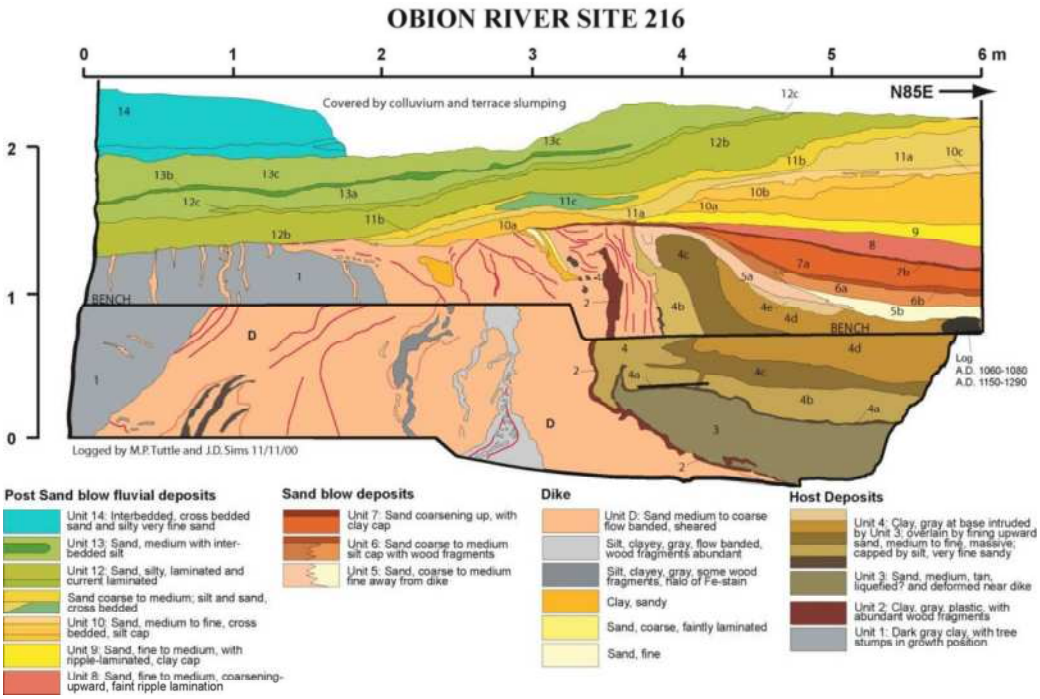

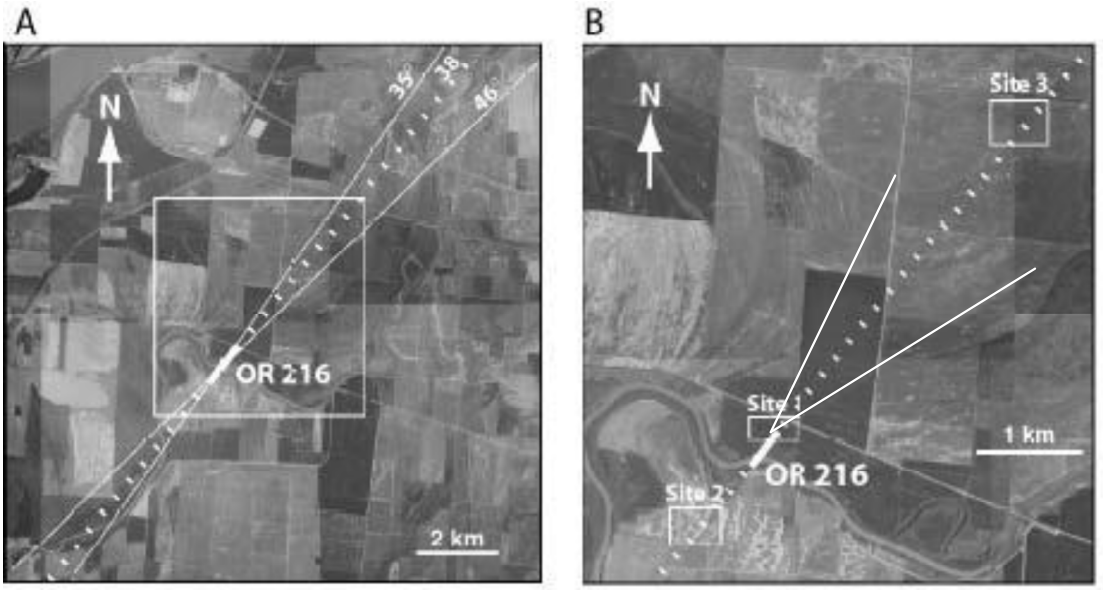

Figure 9: (A): USGS black and white aerial photograph from 1988, with interpreted lineaments based on alignments of sand fissures observed in the photography (overlaid by solid white lines) and on the projection of the hypothesized fault (dashed white line). (B): Magnified white square area of (A). Site 1 corresponds to 2010 summer seismic survey area, while Site 2 refers to potential area that could be used for further seismic exploration (modified from Tuttle and Schweig, 2001).

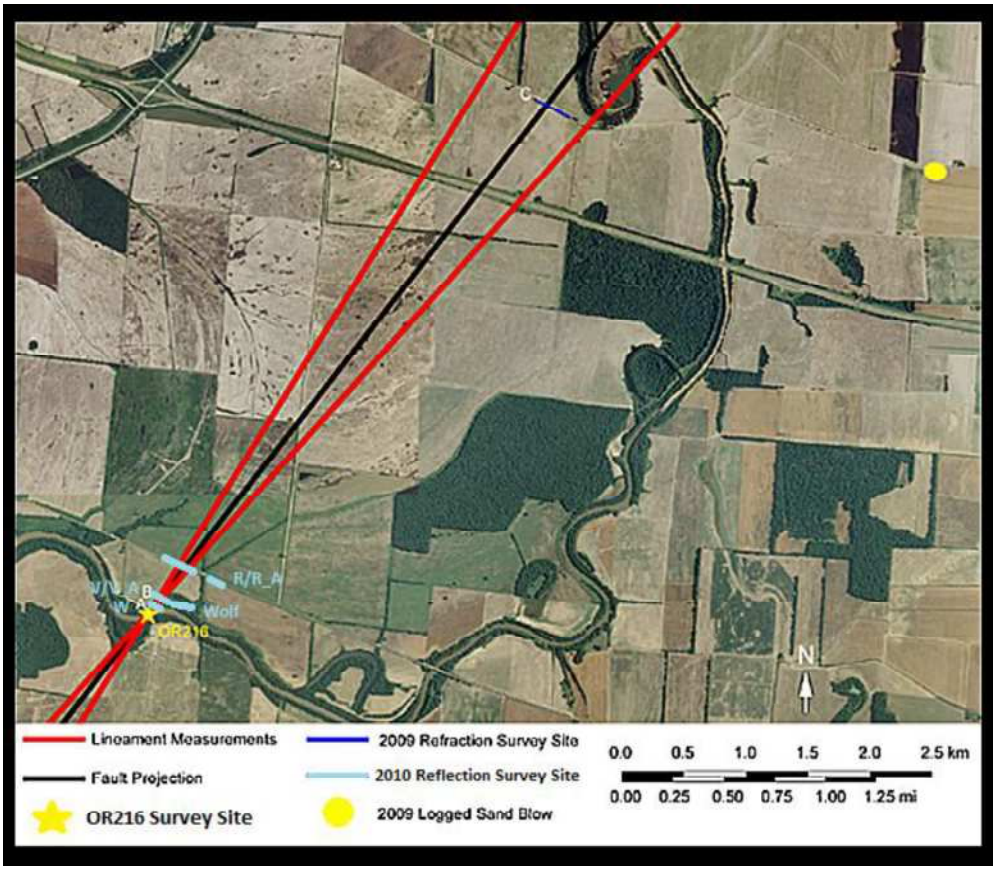

Figure 10: Study area, including the projection of the fault based on previous measurements of the lineament found at OR216, the hypothesized projection of the potential fault (as seen in Figure 9), the four seismic lines collected in the area (R/RA, V/V_A, Wolf, and W), the excavated Lenox Road sand blow, and 2009 seismic refraction survey (A, B, and C).

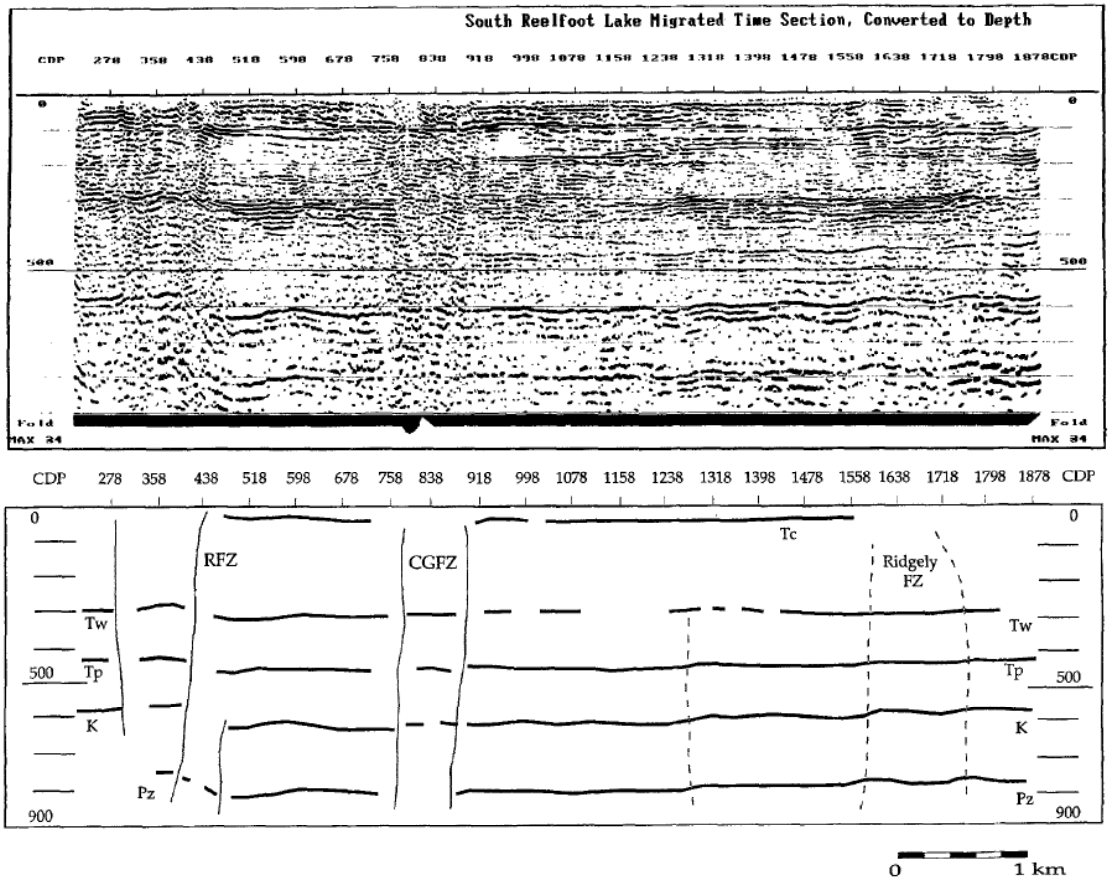

Figure 11: Top: Mini-sosie seismic reflection profile along Reelfoot lake. Bottom: Interpretation of the seismic profile, including geologic unit identification and fault projections. The vertical axis is in meters. RFZ = Reelfoot fault zone, CGF -- Cottonwood Grove fault, Tc = Tertiary Claiborne, Tw = Tertiary Wilcox, Tp = Tertiary Porters Creek, K = Cretaceous, Pz – Paleozoic (from Van Arsdale et al., 1998).

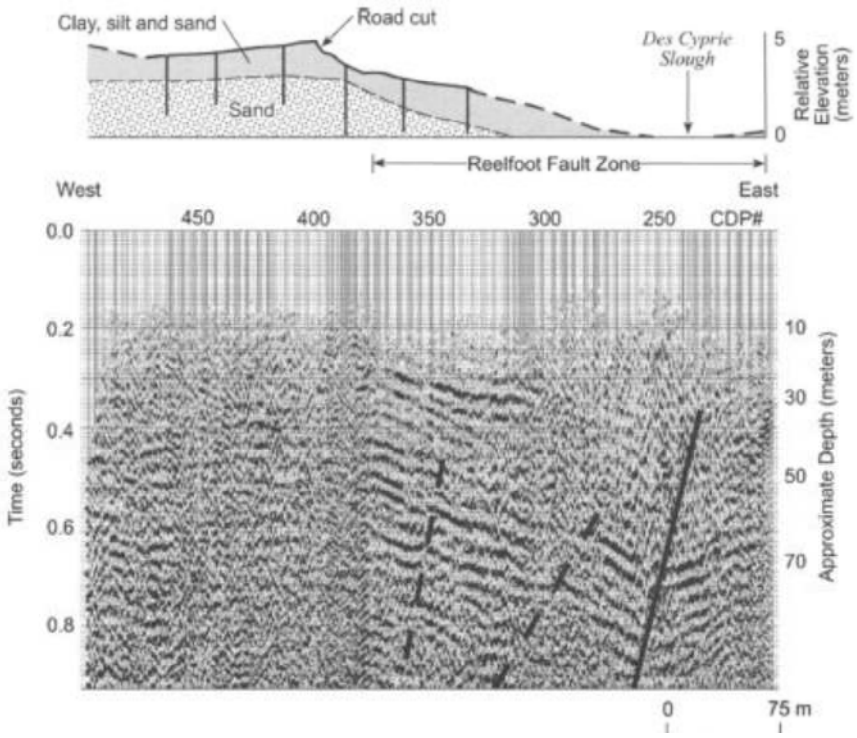

Figure 12: Top: Topographic profile of a survey area west of New Madrid, Missouri. Black lines indicate boreholes (of Van Arsdale et al., 1995). Bottom: Seismic profile of the same area. The solid black line represents primary faulting of the New Madrid North Fault, while the dashed black lines represent secondary extensional faults (from Baldwin et al., 2005).

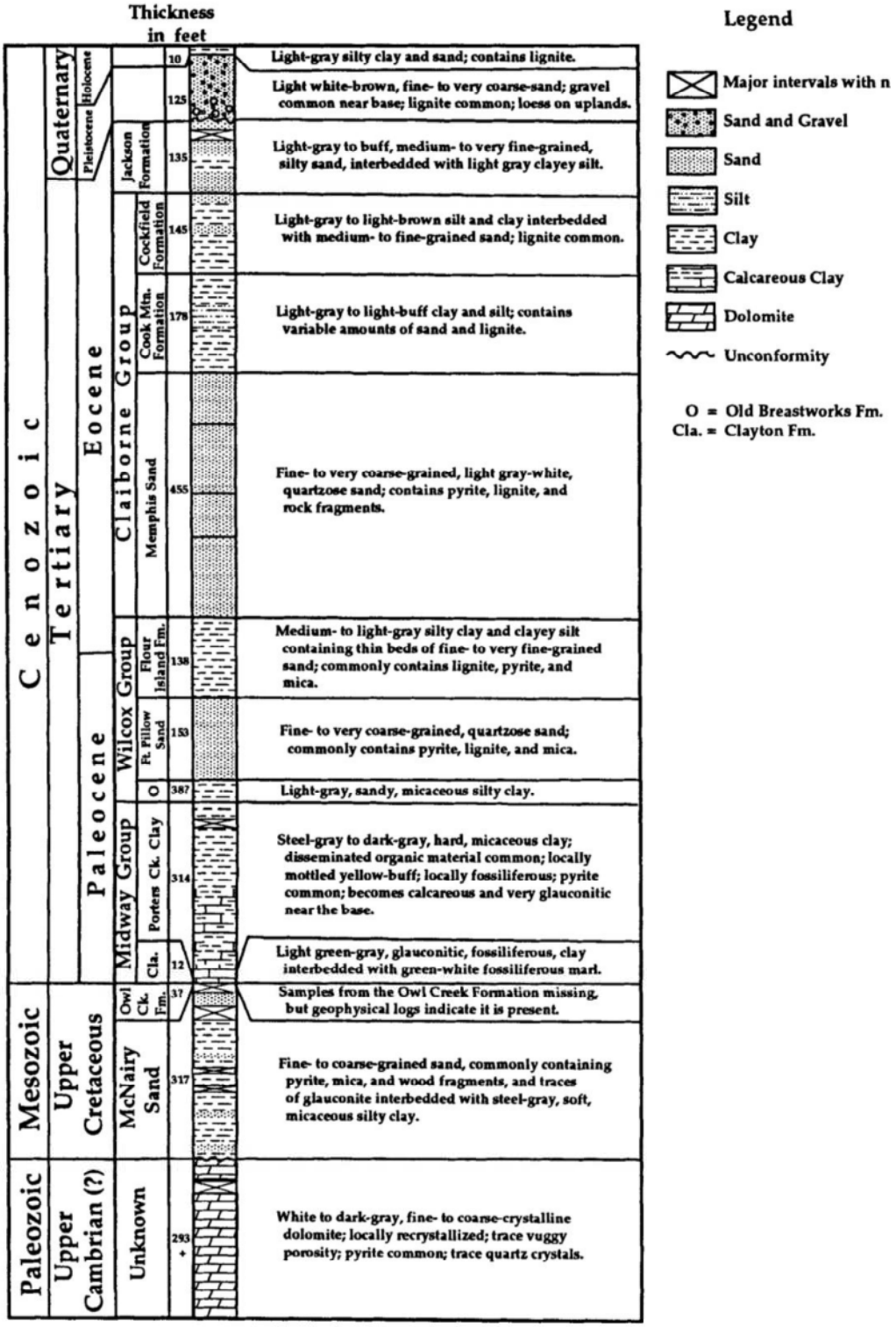

Figure 13: Stratigraphic column of geologic units of the region based on stratigraphy observed at Reelfoot Lake (modified from Van Arsdale and TenBrink, 2000).

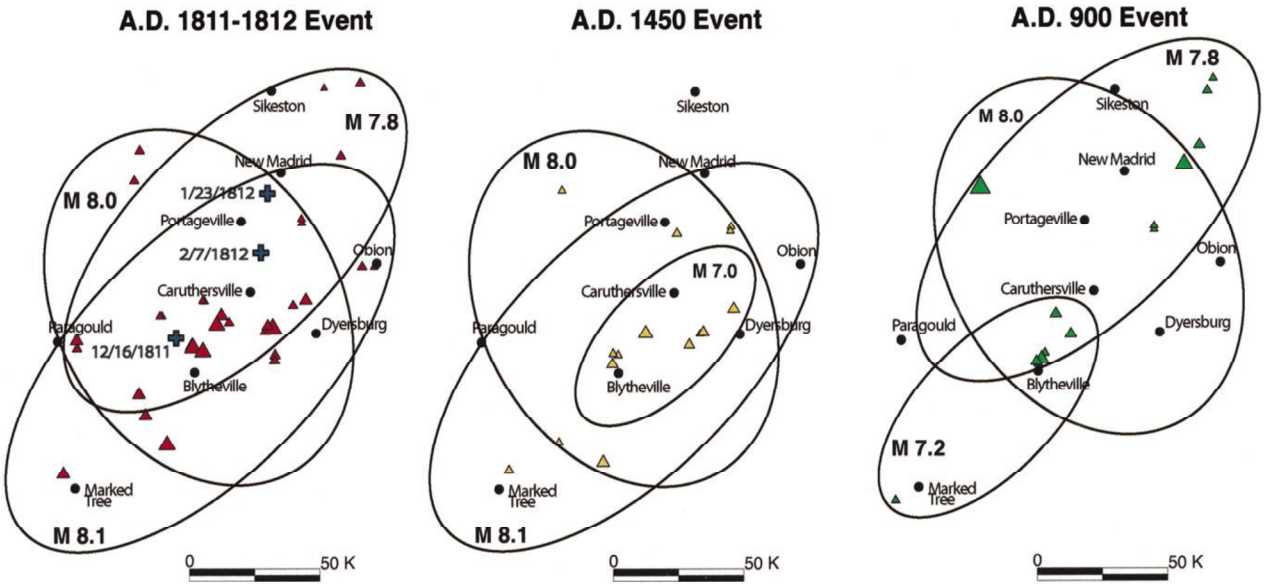

Figure 14: Liquefaction fields for 1811-1812, 1450, and 900 A.D. earthquake events interpreted from the spatial distribution of sand blows, subsurface stratigraphy, and sand blow sizes (from Tuttle et al., 2002).

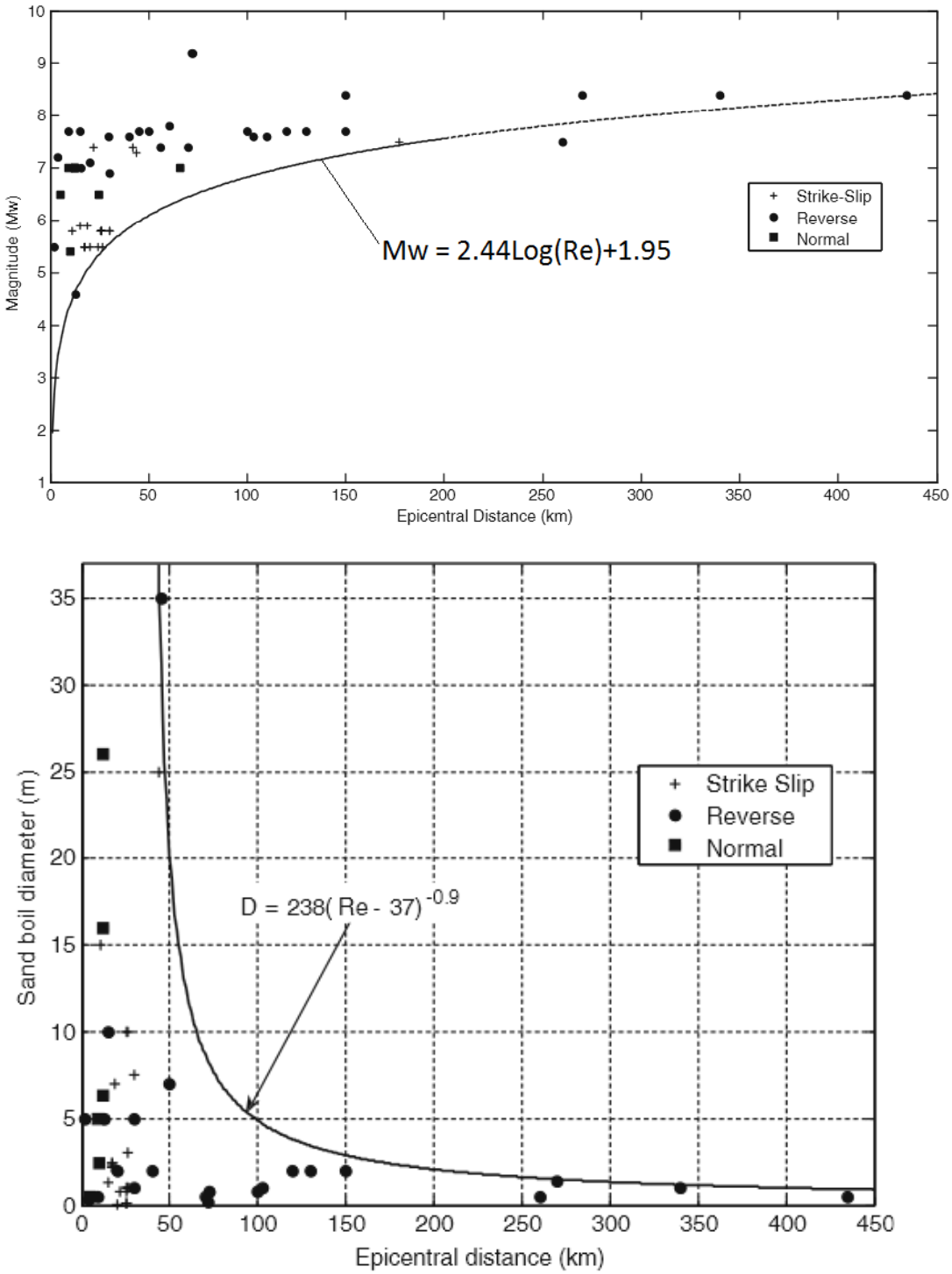

Figure 15: Above: Earthquake magnitude versus sand blow-earthquake distance fit by equation in figure (where Re equals epicenter distance). Below: sand blow (written as "sand boil") diameter versus sand blow-earthquake distance fit by equation in figure (modified from Castilla and Audemard, 2007).

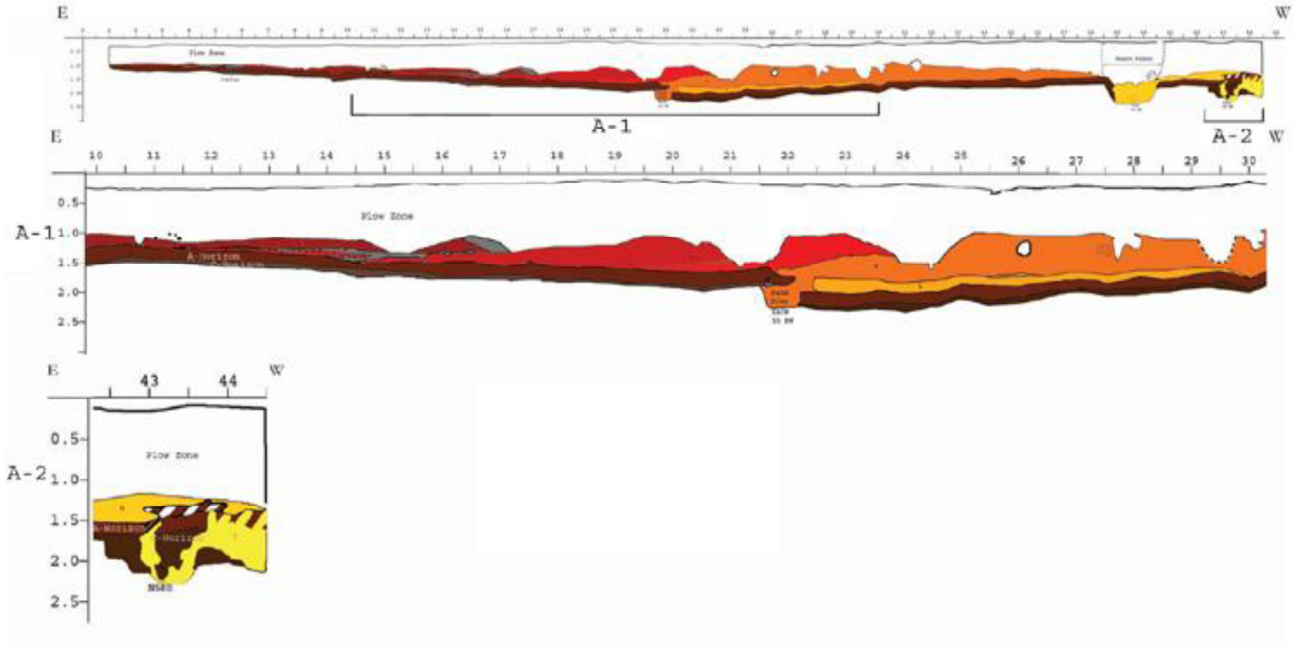
E
W
A-1
A-2
Flow Zone
A-1
A-2
43
44

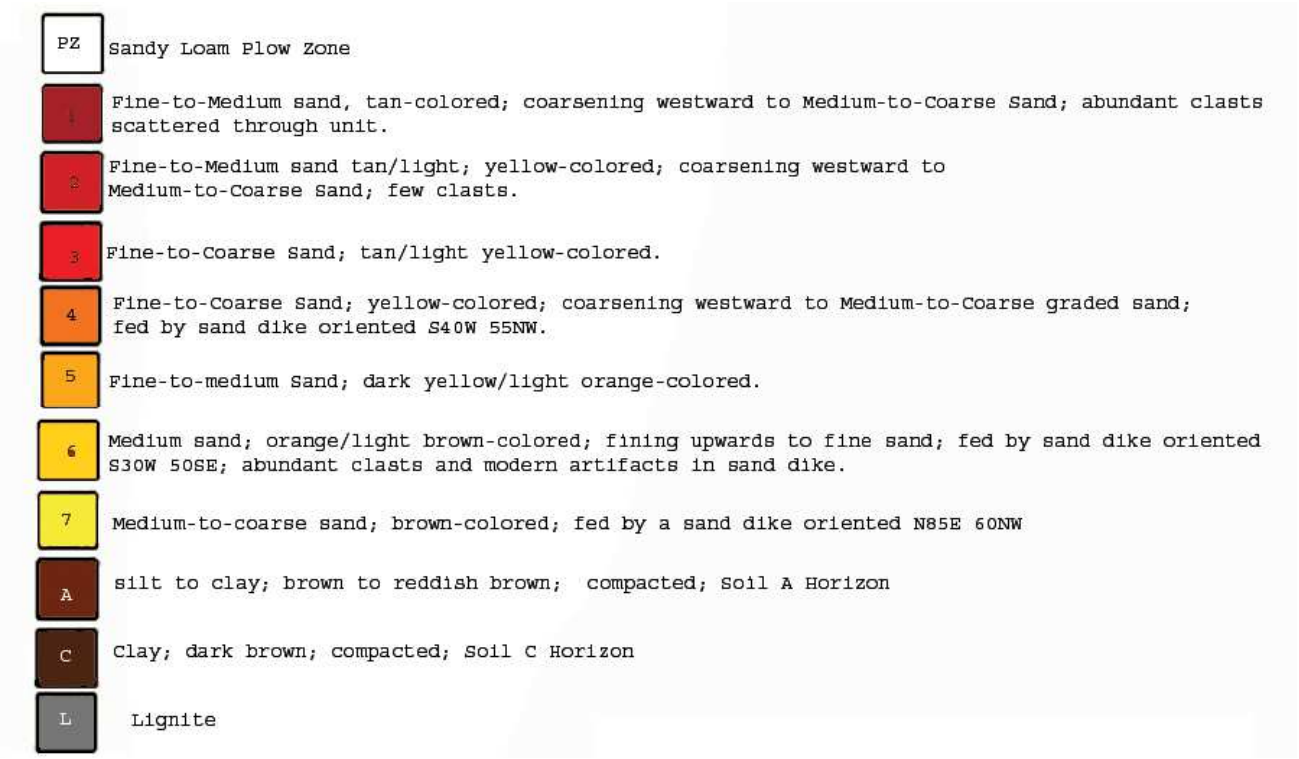

Figure 16: Log of sand blow exposed along Lenox Road near Dyersburg TN, August 2009. Vertical and horizontal scale is in half-meters.

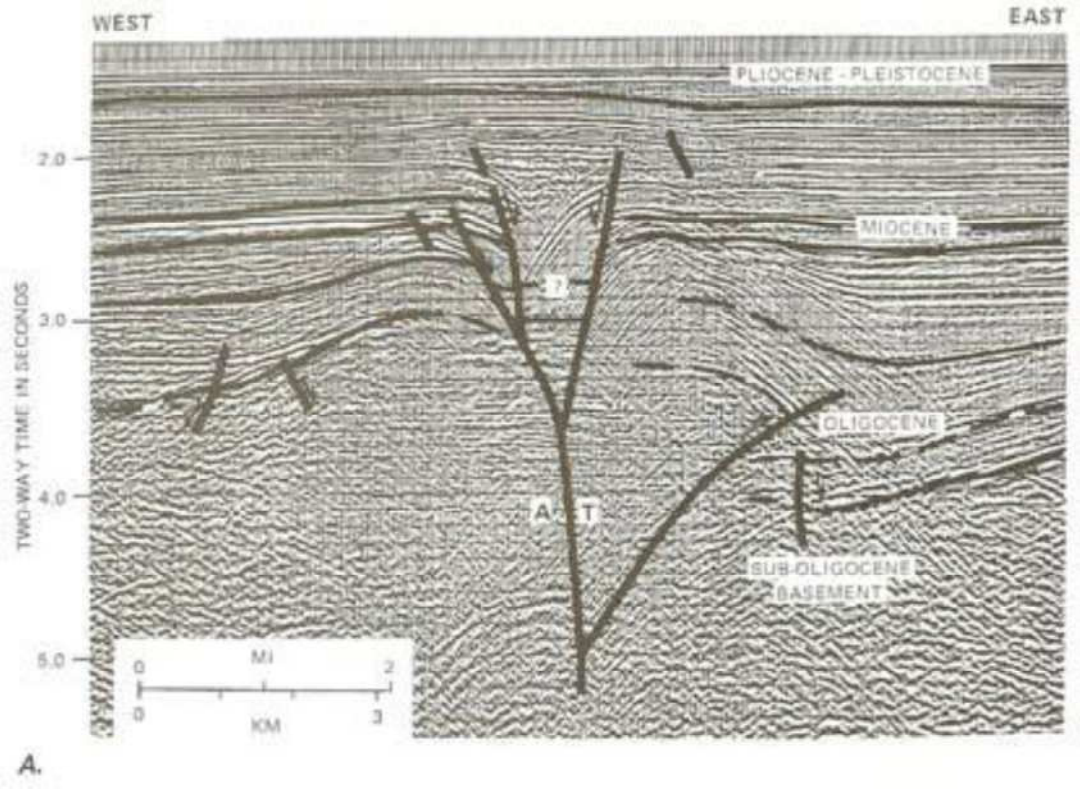

Figure 17: Seismic profile of a flower structure from a dextral strike-slip fault system, the most likely fault structure of the NMSZ for the fault configuration proposed by Tavakoli et al. (2010) and Tuttle and Schweig (2005) (from Harding, 1985)

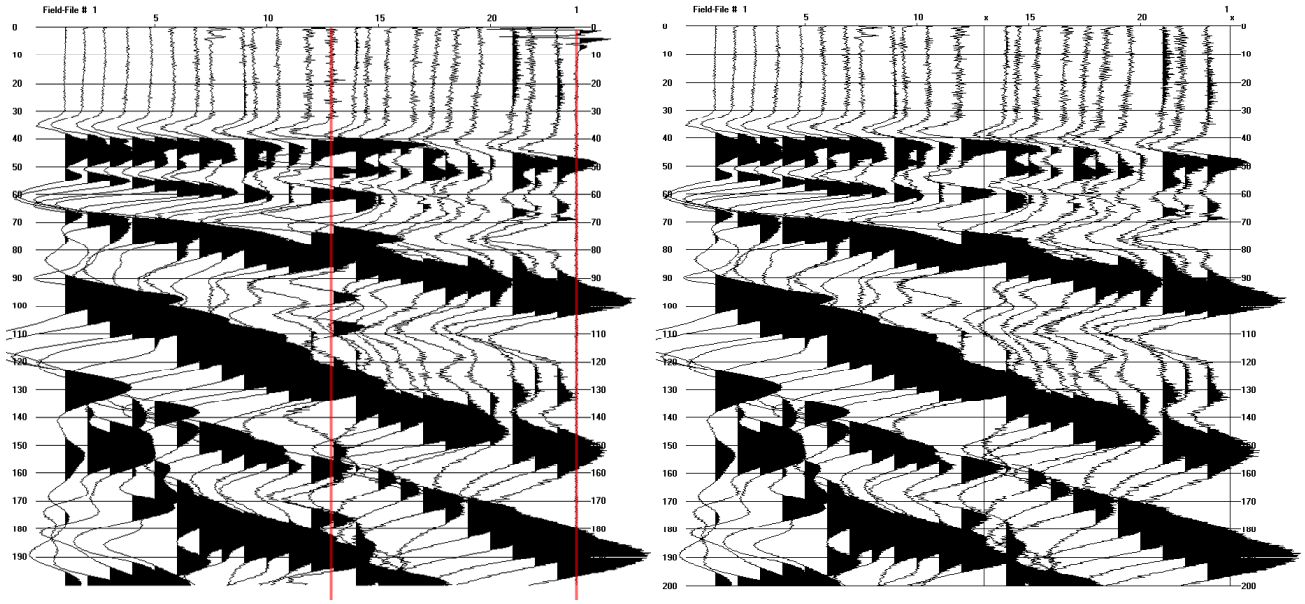

Figure 18: Left: An initial shot-gathered section from line W after conversion to KSG format. Noisy/flat traces related to geophone malfunction in the field are indicated by the red line through the geophone channel. Right: Same section after highlighted traces in the plot at left are killed.

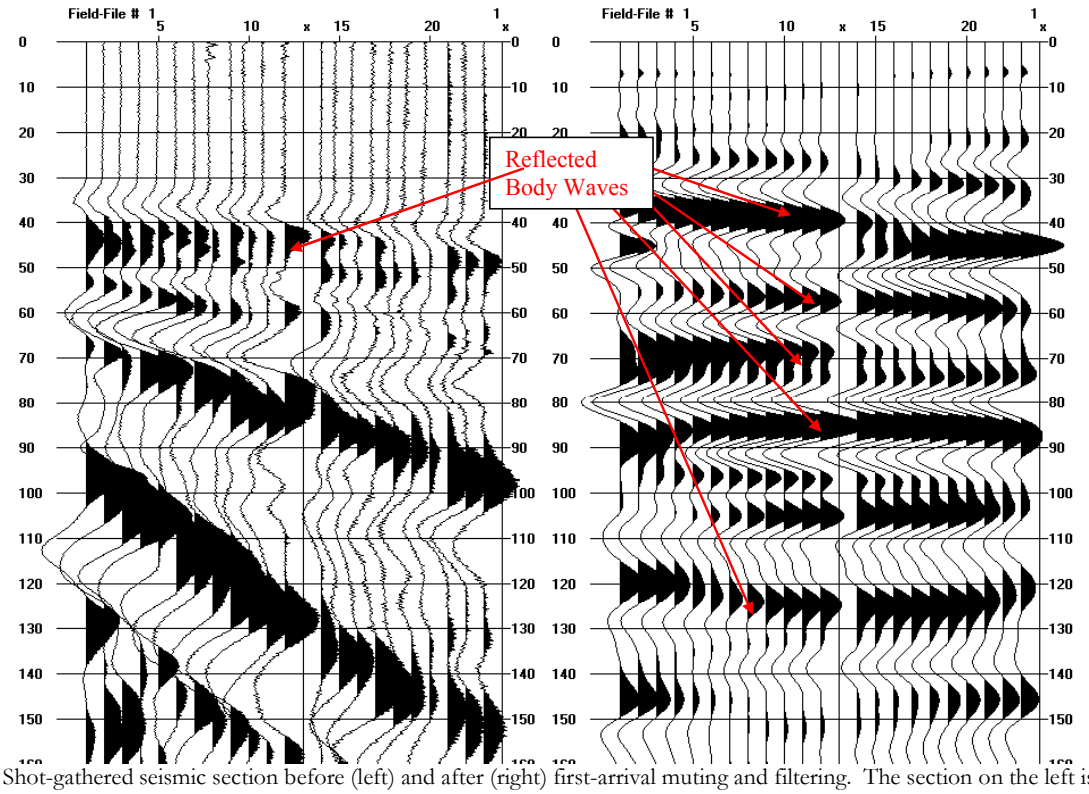

Figure 19: Shot-gathered seismic section before (left) and after (right) first-arrival muting and filtering. The section on the left is dominated by surface waves, obscuring possible reflected body waves; more reflected body waves are visible after the muting and filtering.

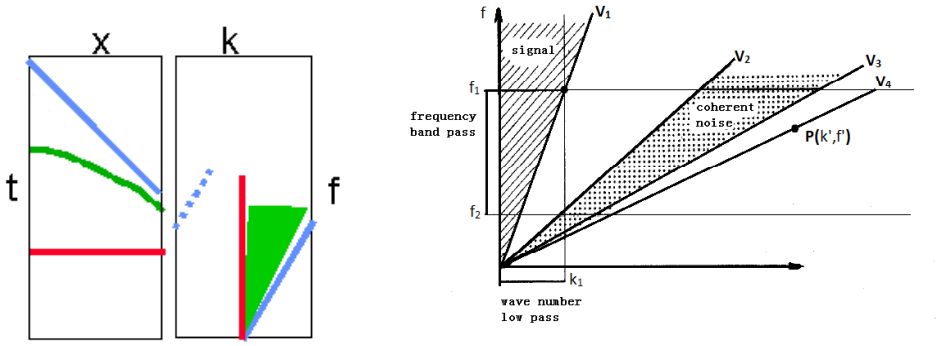

T = Time X = Distance/Depth F = Frequency K = Wavenumber

Figure 20: Left: Basic correlation of T-X (time-domain) space and F-K (Frequency-wavenumber) space. The wave energy (green line) travels in a curved line in T-X space and falls between the maximum (blue line) and minimum (red line) filter bands. When converted to F-K space, the waveform covers a larger area of potential values within the filter bands (from Hardy, 2008). Right: Practical example of the use of F-K filtering. Velocities between V2 and V3 represents a range of coherent noise that needs to be eliminated to improve the quality of the processed data that would be eliminated through F-K filtering (from ChaseBilleaudeau, 2012).

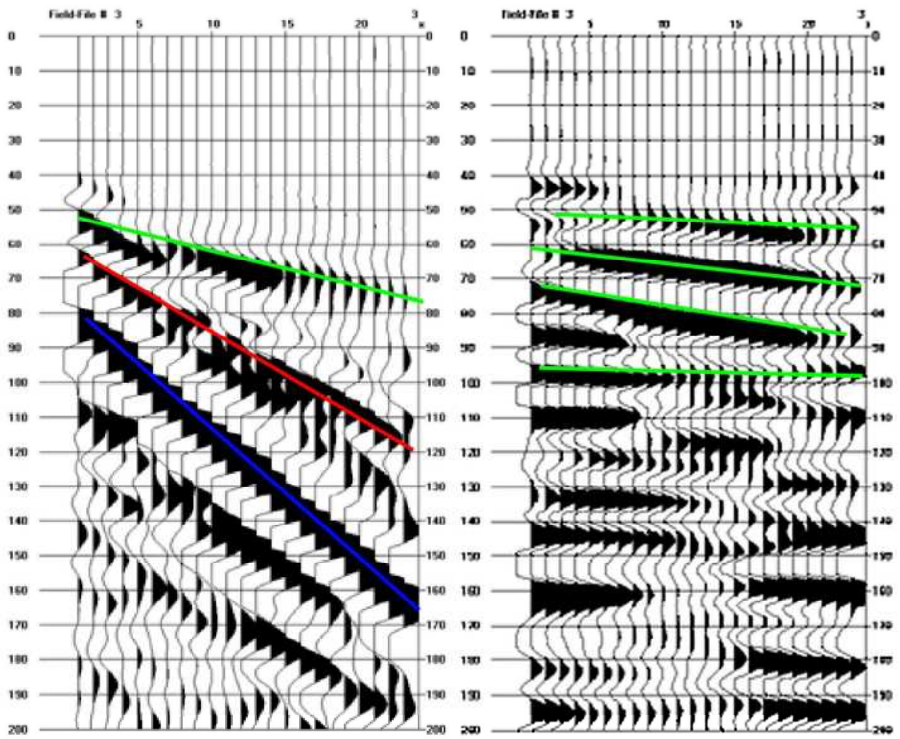

Figure 21: Left: Unfiltered shot gather. A possible reflector (green) is observed, but slower surface waves (red) and air waves (blue) obscure any reflectors at depth. Right: Same section put through a band-pass and F-K filter. Slower, lower frequency seismic waves are filtered out, leaving only near-horizontal reflectors.

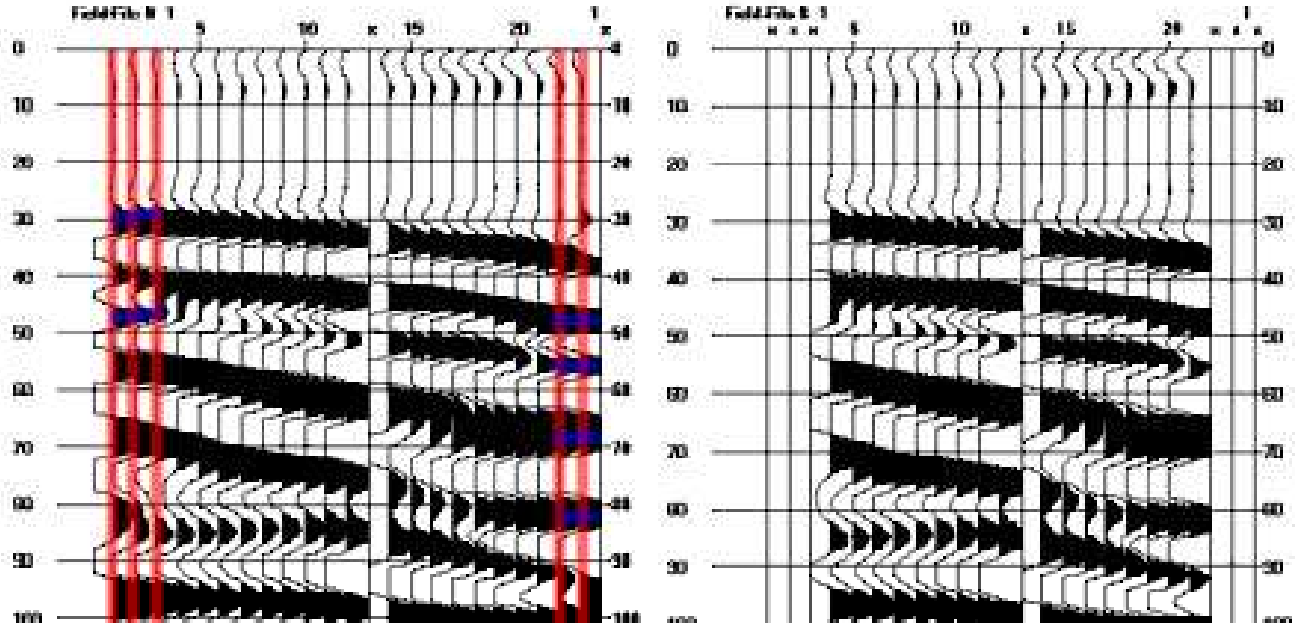

Figure 22: Left: Reflectors showing negative moveout in arrival times at the beginning (left side) of the section and no moveout towards the end (right side) of the section (highlighted in blue), the result of programming errors within WinSeis based on discussions with the Kansas Geological Survey. Any traces with such arrival time trends (highlighted in red) are killed. Right: Same section after highlighted traces are killed (muted).

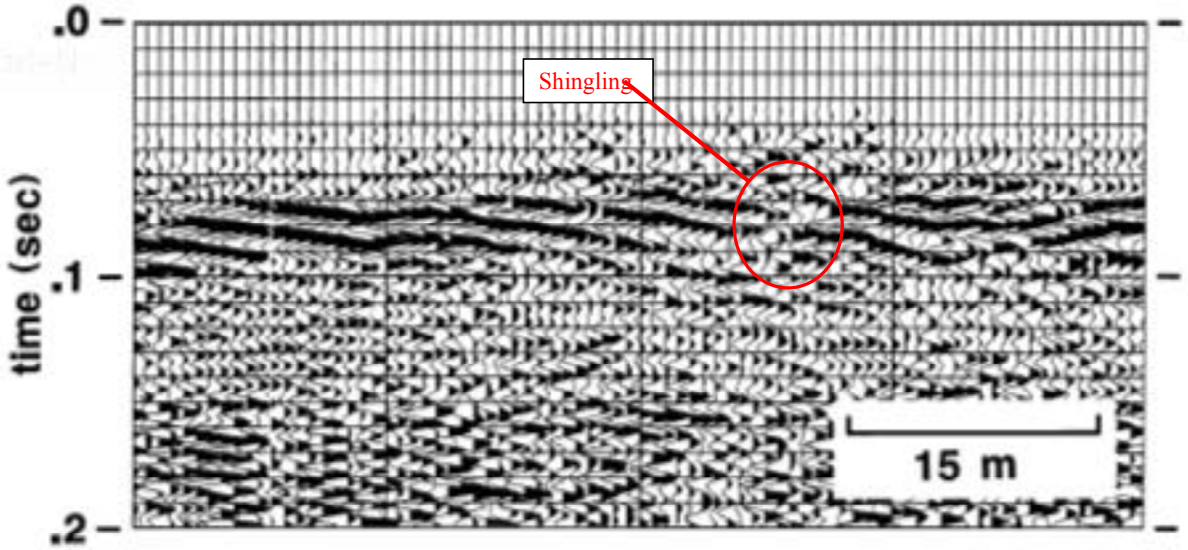

Figure 23: Example of shingling in a seismic section (from Steeples and Miller, 1998).

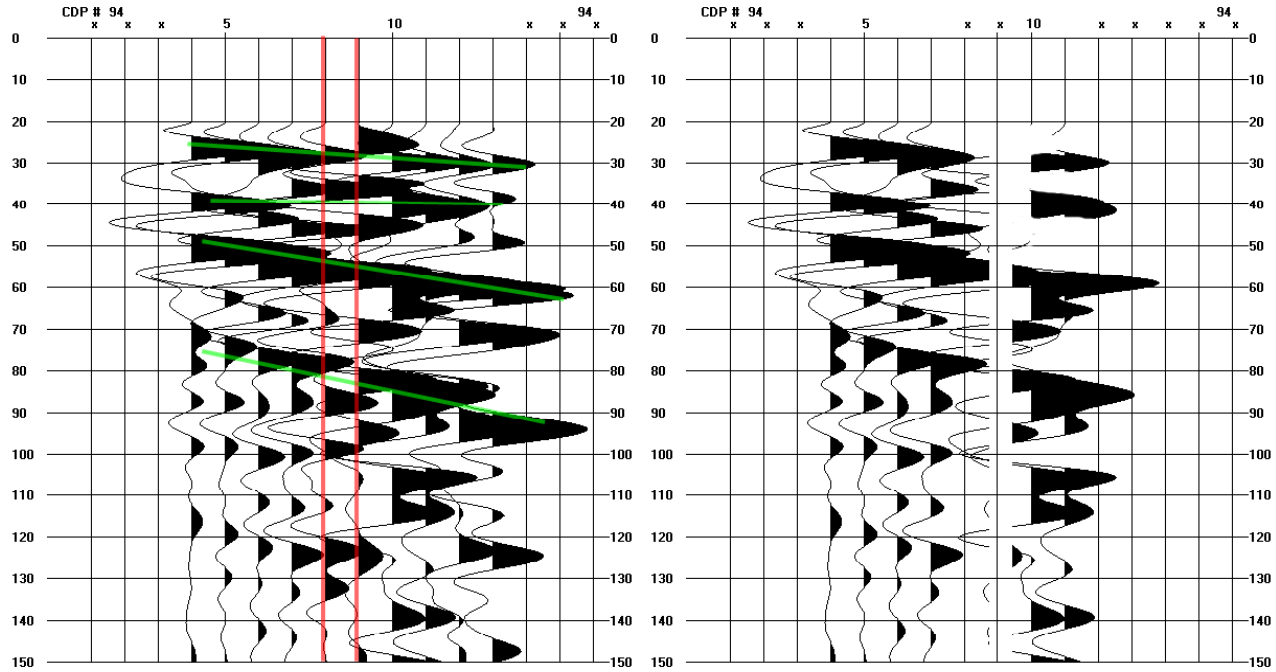

Figure 24: Left: CDP-sorted section with lines drawn through the peaks of waves of possible reflectors (highlighted in green). Traces that caused shingling in the stacked section (highlighted in red) were killed. Right: Same section after highlighted traces were killed.

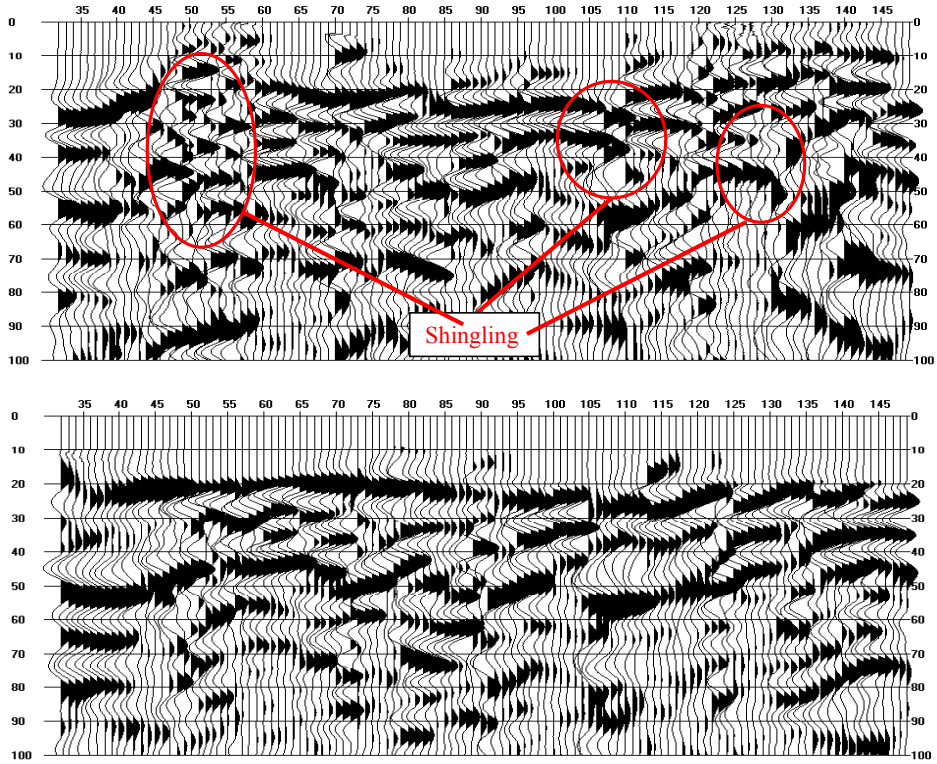

Figure 25: Stacked seismic section before (top) and after (bottom) killing traces in CDP-gathered section. While some shingling remains in the section, the majority of the shingling has been eliminated.

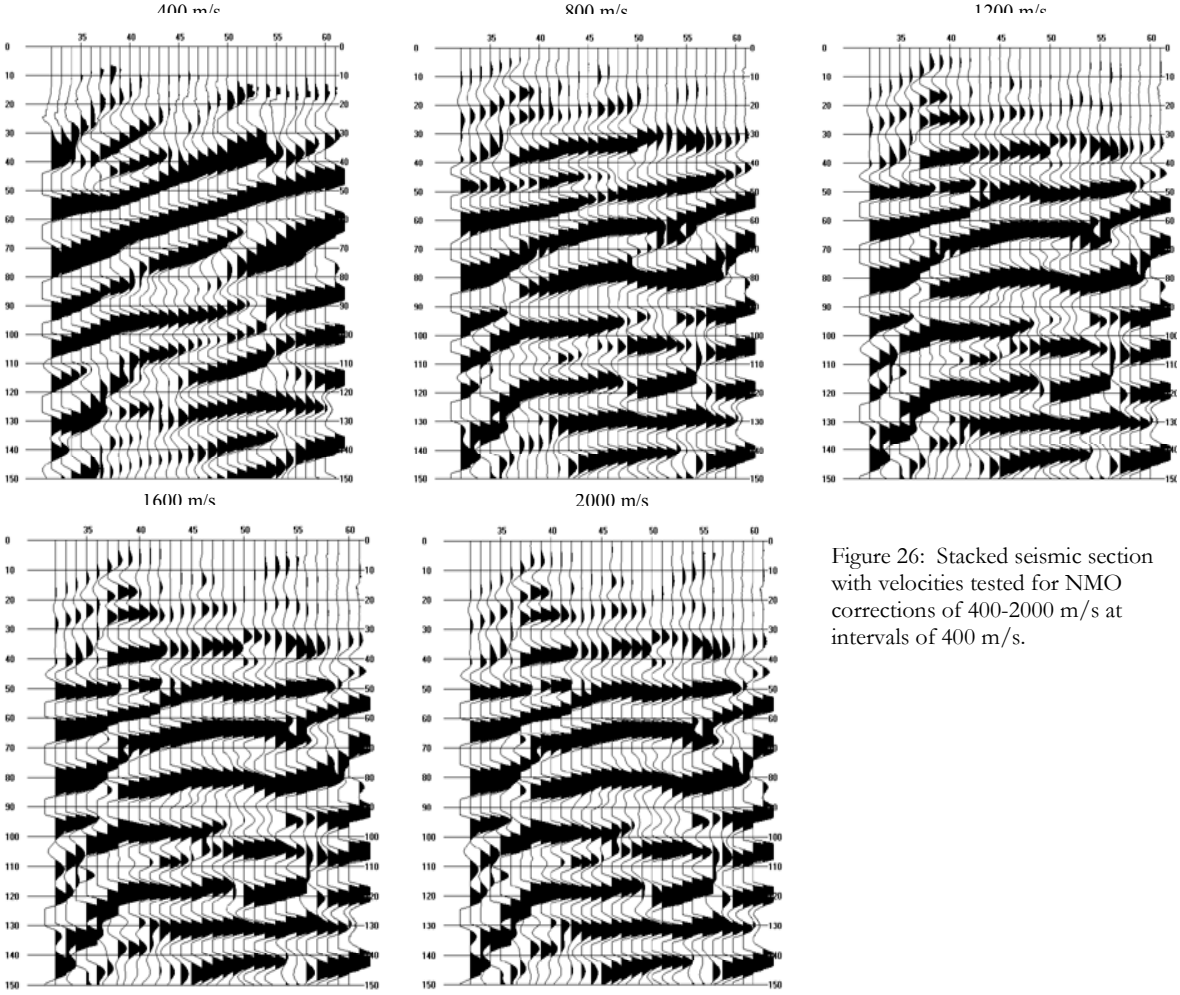

Figure 26: Stacked seismic section with velocities tested for NMO corrections of 400-2000 m/s at intervals of 400 m/s.

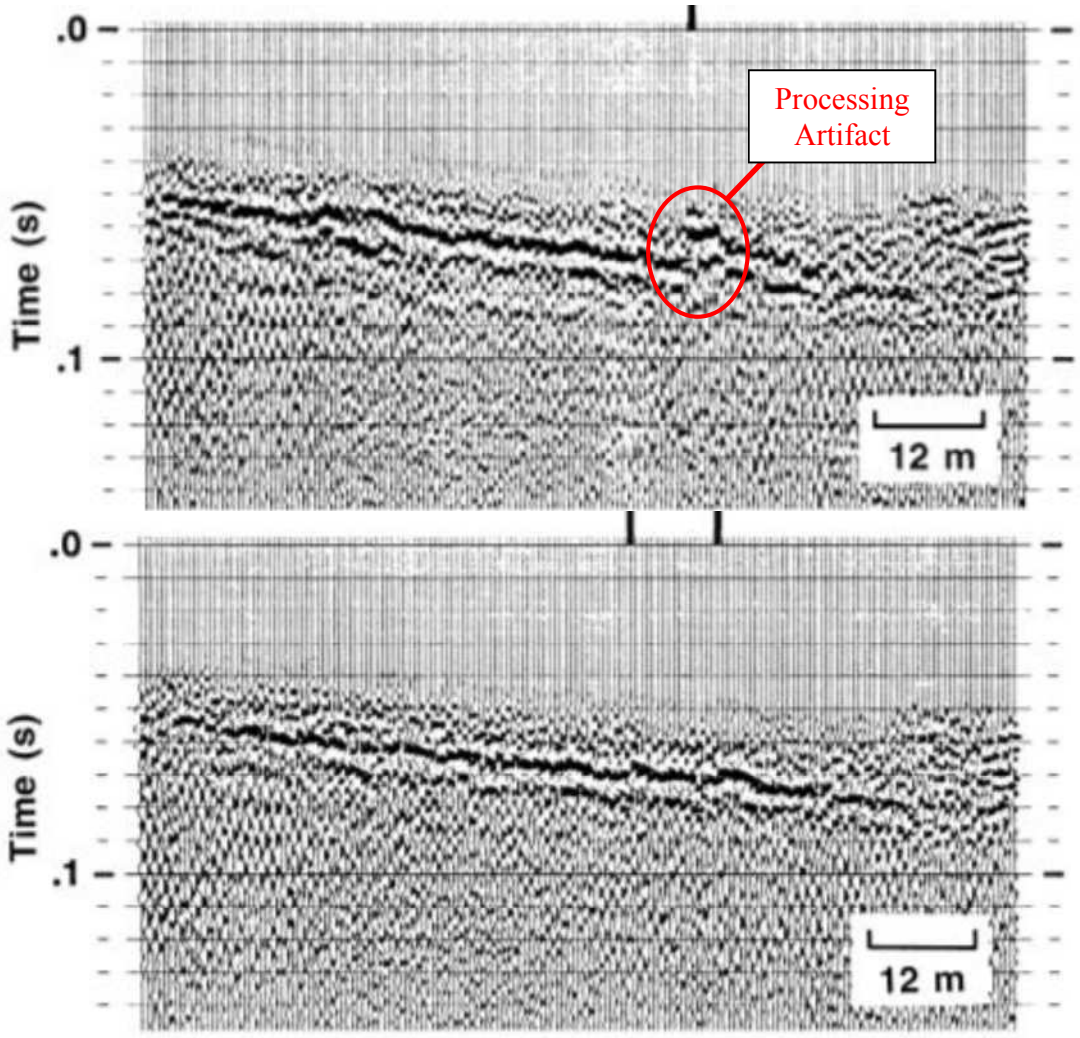

Figure 27: Top: Example stacked seismic section with a processing artifact. An apparent fault (highlighted) is actually an artifact of incorrect stacking velocity. Below: Same seismic section after correct stacking velocity is applied (modified from Steeples and Miller, 1998)

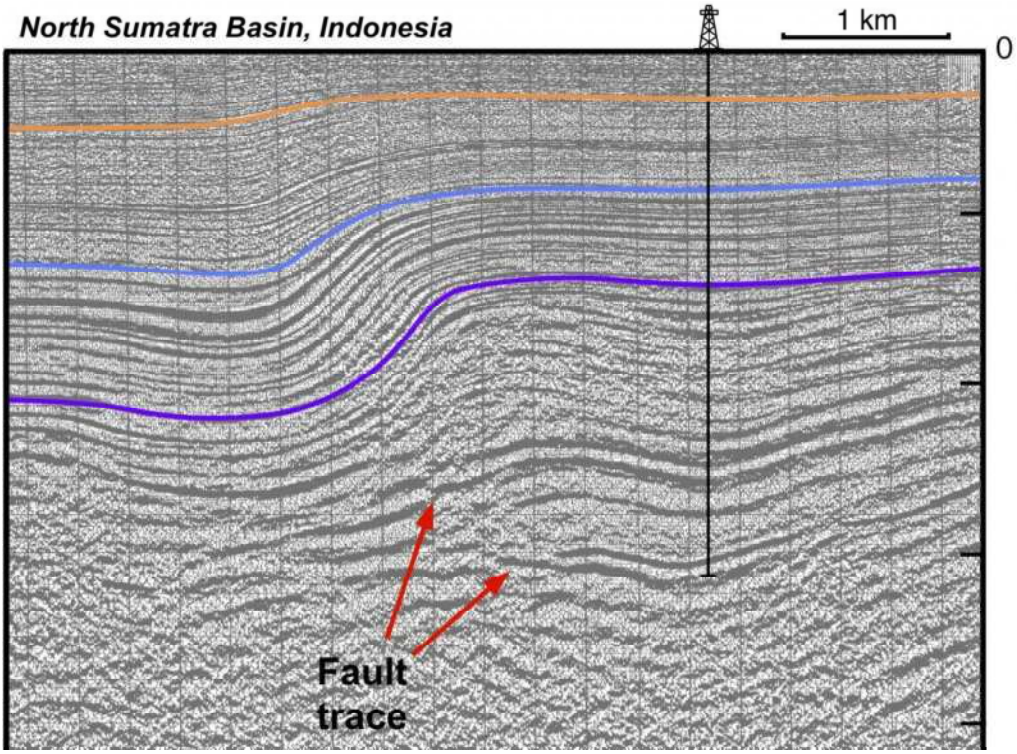

Figure 28: Example of a strike-slip fault at depth in a seismic reflection profile (modified from Shaw et al., 1997).

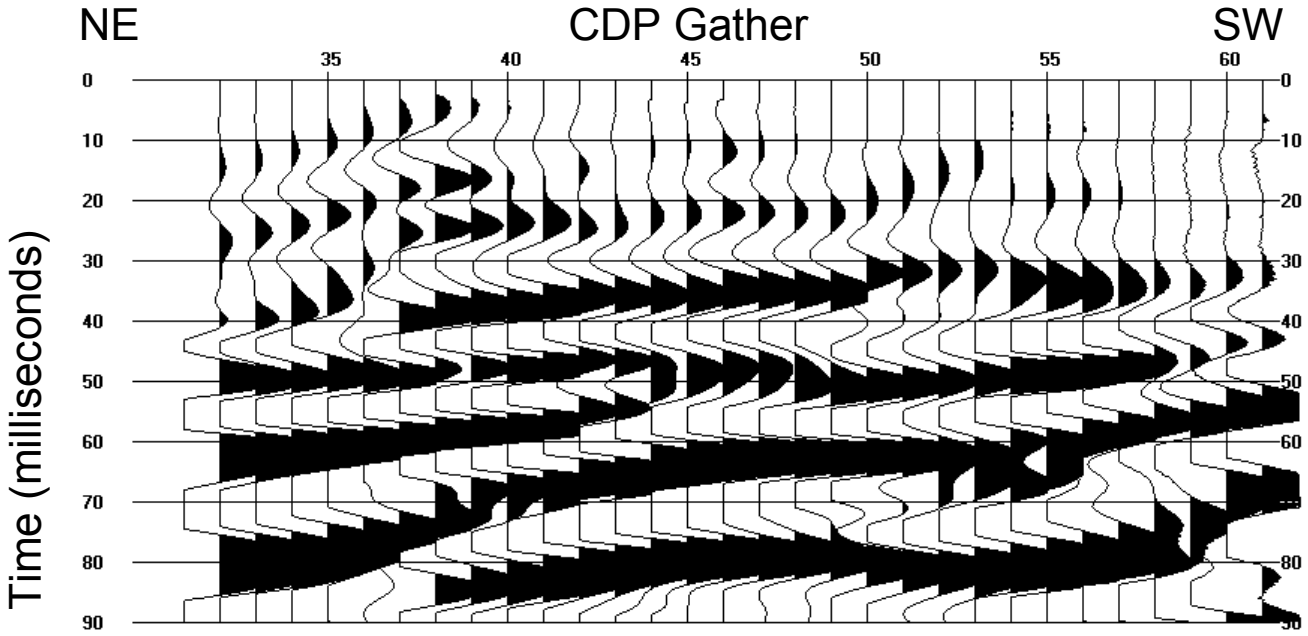

Figure 29: Fully processed 2010W seismic section.

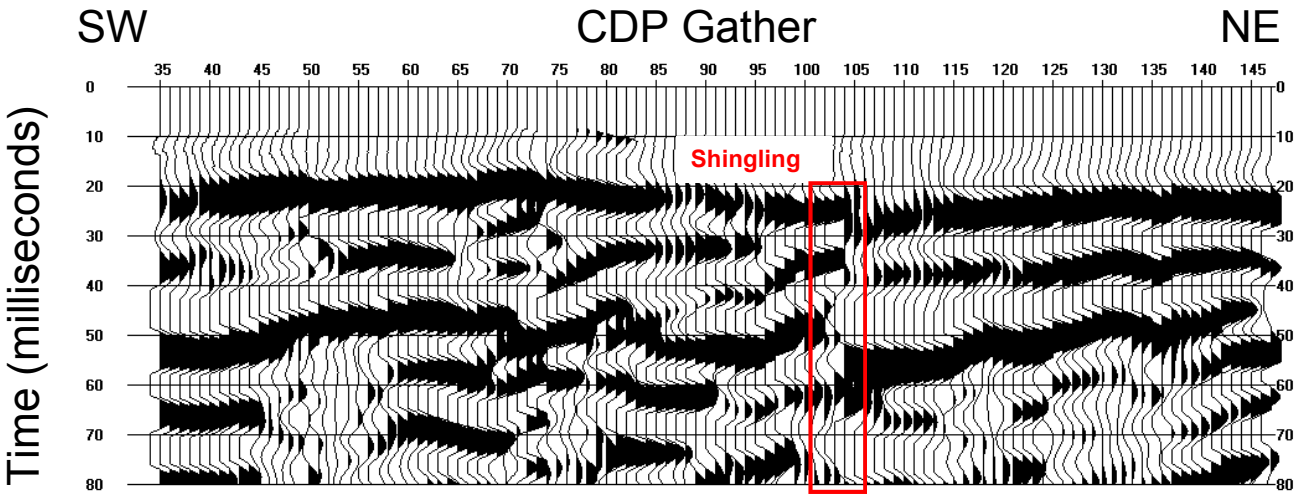

Figure 30: Fully processed 2010V seismic section. Shingling identified in red.

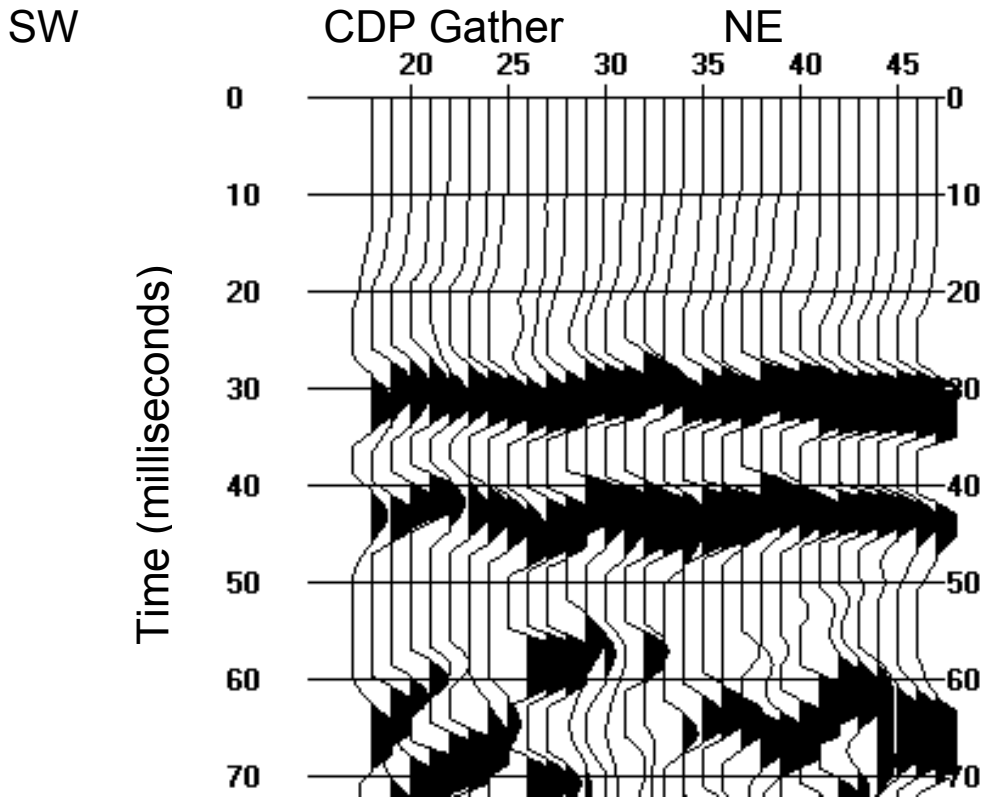

Figure 31: Fully processed 2010V_A seismic section.

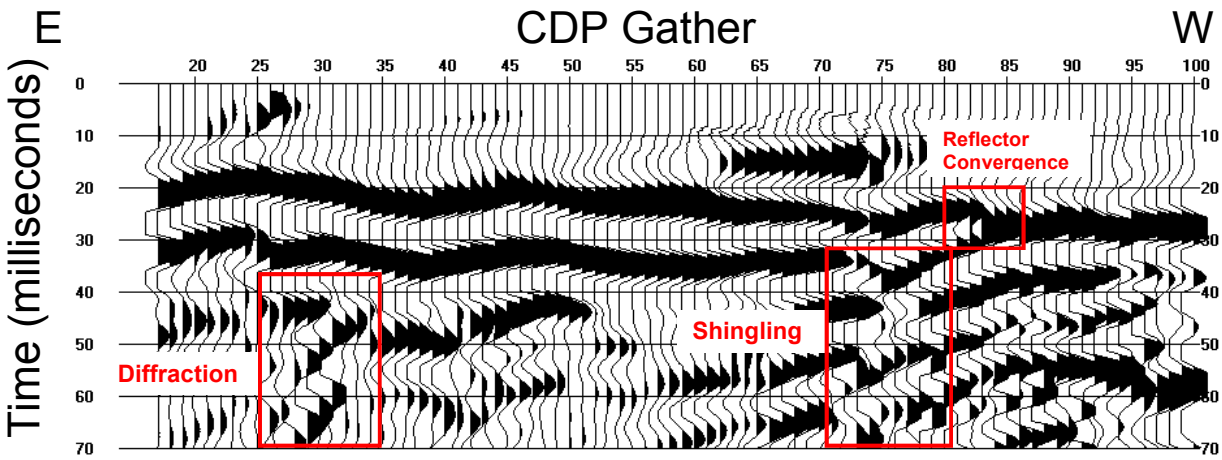

Figure 32: Fully processed R seismic section. Shingling, convergence of reflectors, and diffraction are identified in red.

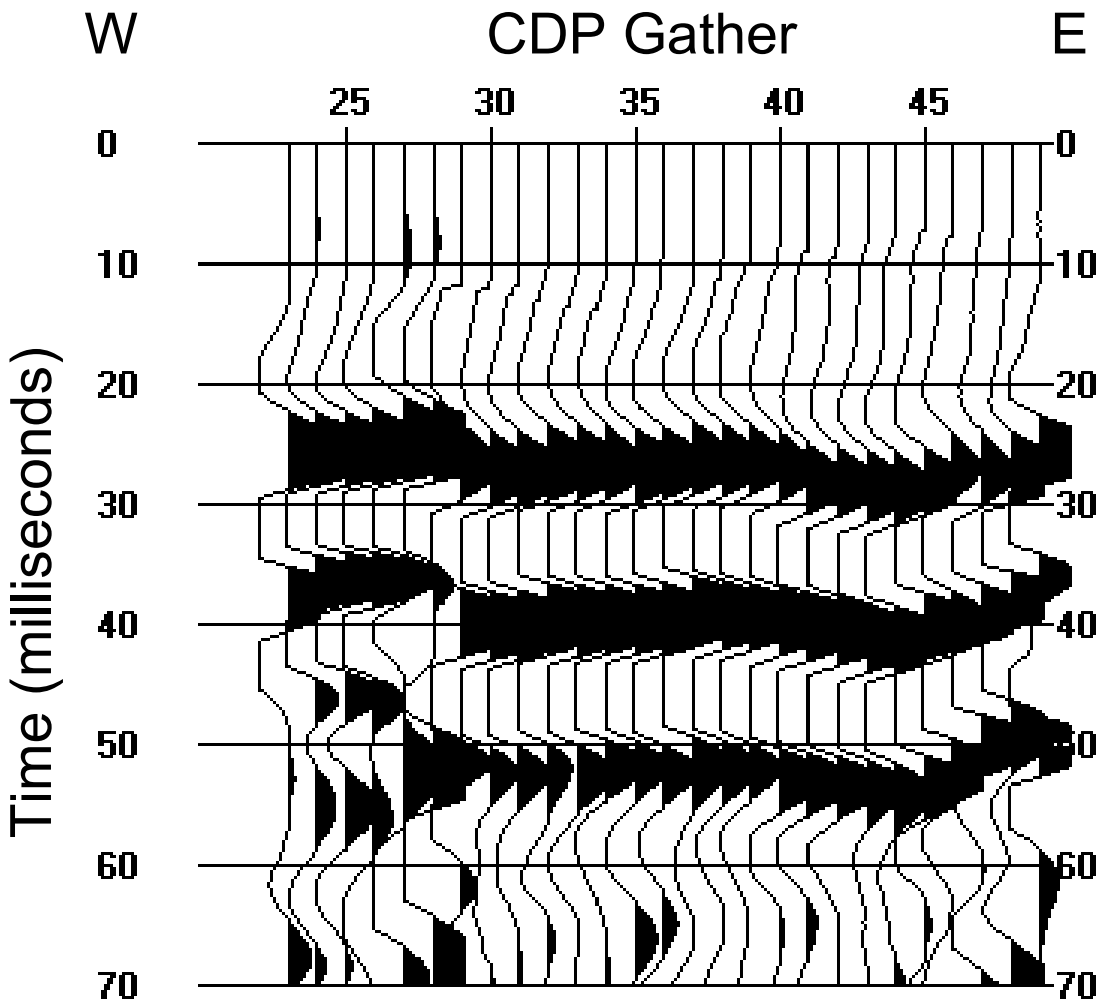

Figure 33: Fully processed 2010R_A seismic section.

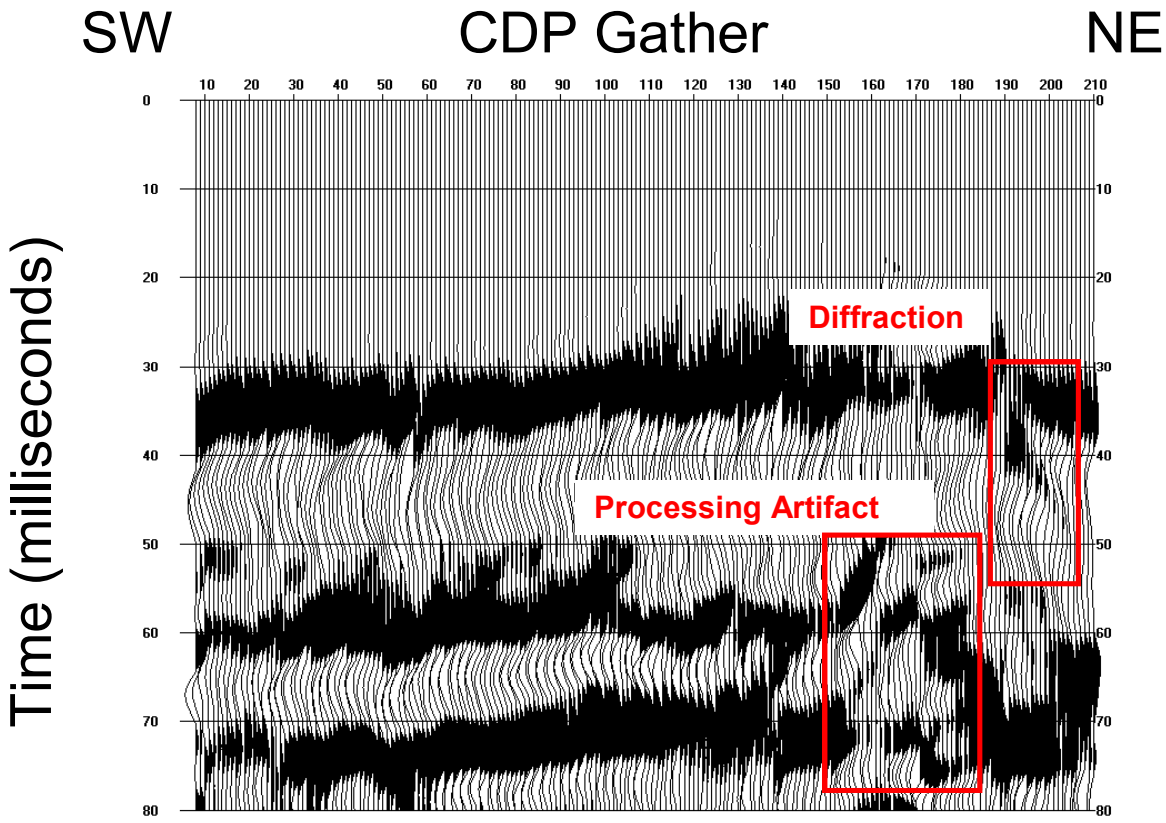

Figure 34: Fully processed Wolf seismic section. Processing artifact caused by switch in shot-gather method and diffractions identified in red.

Table 1						
Data acquisition parameters for the seismic-reflection survey						
Seismic Line	OR216-R	OR216-RA	OR216-V	OR216-VA	OR216-W	Wolf
Source	12 kg slegehammer	12 kg sledgehammer	12 kg slegehammer	12 kg slegehammer	12 kg slegehammer	12 kg sledgehammer
Source Spacing	1 m to 12 m	1 m to 12 m	0.5 to 12 m	1 m to 12 m	0.5 m to 9 m	10 m to 12 m
Receivers	28 Hz vertical geophones	28 Hz vertical geophones	28 Hz vertical geophones	28 Hz vertical geophones	28 Hz vertical geophones	
Receiver Spacing	1 m	1 m	1 m	1 m	.5 m	2 m
Spread Configurations	Off-end	Off-end	Off-end	Off-end	Off-end	Off-end to split
Recording System	RAS-24 (24 Channels)	RAS-24 (24 Channels)	RAS-24 (24 Channels)	RAS-24 (24 Channels)	RAS-24 (24 Channels)	
Minimum Fold	6	6	6	6	6	6
Record Length	4000 ms	4000 ms	4000 ms	4000 ms	4000 ms	1000 ms
Digitization Interval	.125 ms	.125 ms	.125 ms	.125 ms	.125 ms	.125 ms
First Arrival Mute	20 ms	20 ms	20 ms	10 ms	20 ms	20 ms
Band pass Filter Length	100-150 ms	100-150 ms	100-150 ms	100-150 ms	100-150 ms	100-150 ms
F-K Filter Slope Cutoff (ms/trace)	.6	.4	.4	.4	.3	.3

Table 2
Standard procedure for the processing seismic-reflection profiles
Processing Steps
1. KSG Data Conversion
2. Initial Trace Kill
3. Surgical mute of field traces
4. Band-pass Period filter
5. F-K Zero-slope filter
6. Surgical mute in shot gather
7. Resort to CMP gather
8. Surgical mute in CMP gather
9. NMO Correction
10. Automatic Gain Control
11. Velocity Stack

Appendix A: Seismic Reflection Processing Tables

How to read tables: When referring to "first trace" and "last trace" within a shot gather or CDP gather mute, the extent of the mute covers the range of the first and last trace and excludes all other traces in that gather. In this example:

Shot-Gather	First Trace Killed	Last Trace Killed	First Trace Killed	Last Trace Killed
1	1	3	22	24

For shot gather 1, traces 1 through 3 were completely muted and traces 22 through 24 were completely muted. All other traces in that shot gather were not muted.

In this example:

Shot-Gather	First trace	Mute (ms)	Last Trace	Mute (ms)
1	1	30	24	59

Traces 1-24 had first arrival mutes. Trace 1 had the first arrival mute extend to 30 ms, while trace 24 had the first arrival mute extend to 59 seconds. Traces in between were muted in a linear fashion, so the muted section of each trace between traces 1 and 24 increased by 1.208 ms, or (59-30)/24 ms.

Step 3 First Arrival Mute values

Survey Line	First arrival Mute	Taper Length
W	20 ms	2 ms
V	20 ms	2 ms
VB	10 ms	2 ms
R	20 ms	0 ms
RB	20 ms	0 ms
Wolf	See detailed Mute Schedule	1 ms

Step 3 Mute Schedule for Wolf seismic survey line

Shot-Gather	1st trace	Mute (ms)	24th Trace	Mute (ms)
1	1	30	24	59
2	1	30	24	59
3	1	30	24	59
4	1	30	24	59
5	1	30	24	59
6	1	30	24	59
7	1	30	24	59
8	1	30	24	59
9	1	30	24	59
10	1	30	24	59
11	1	30	24	59
12	1	30	24	59
13	1	30	24	59
14	1	30	24	59
15	1	30	24	59
16	1	30	24	59
17	1	30	24	59
18	1	30	24	59
19	1	30	24	59
20	1	30	24	59
21	1	30	24	59
22	1	30	24	59
23	1	30	24	59
24	1	30	24	59
25	1	30	24	59
26	1	30	24	59
27	1	30	24	59
28	1	30	24	59
29	1	30	24	59
30	1	30	24	59
31	1	30	24	59
32	1	30	24	59
33	1	30	24	59
34	1	30	24	59
35	1	30	24	59
36	1	30	24	59
37	1	30	24	59
38	1	30	24	59
39	1	30	24	59
40	1	30	24	59

Shot-Gather	First trace	Mute (ms)	Last Trace	(Mute)
41	1	30	24	59
42	1	30	24	59
43	1	30	24	59
44	1	30	24	59
45	1	30	24	59
46	1	30	24	59
47	1	30	24	59
48	1	28	24	56
49	1	28	24	56
50	1	28	24	56
51	1	28	24	56
52	1	28	24	56
53	1	28	24	56
54	1	28	24	56
55	1	28	24	56
56	1	28	24	56
57	1	28	24	56
58	1	28	24	56
59	1	28	24	56
60	1	28	24	56
61	1	28	24	56
62	1	28	24	56
63	1	28	24	56
64	1	28	24	56
65	1	28	24	56
66	1	28	24	56
67	1	28	24	56
68	1	28	24	56
69	1	28	24	56
70	1	28	24	56
71	1	28	24	56
72	1	28	24	56
73	1	28	24	56
74	1	28	24	56
75	1	28	24	56
76	1	26	24	51
77	1	25	24	51
78	1	23	24	49
79	1	23	24	49
80	1	22	24	47
81	1	21	24	45
82	1	21	24	46
83	1	19	24	45
84	1	18	24	44
85	1	17	24	43
86	1	16	24	41
87	1	15	24	40
88	1	14	24	39
89	1	65	47	8
90	1	62	47	8
91	1	63	47	9
92	1	64	47	10
93	1	65	47	11

Shot-Gather	First trace	Mute (ms)	Last Trace	(Mute)
94	1	66	47	13
95	1	67	47	14
96	1	68	47	15
97	1	70	47	16
98	1	71	47	17
99	1	72	47	18
100	1	73	47	19
101	1	74	47	20
102	1	75	47	22
103	1	76	47	23
104	1	77	47	24
105	1	79	47	25
106	1	80	47	26
107	1	81	47	27
108	1	82	47	28

Step 4 band-pass filter corner values

Survey Line	Low-Cut Corner Frequency (Hz)	High-Cut Corner Frequency (Hz)	Filter Length (points)
W	80	150	71
V	70	150	91
VB	80	150	91
R	100	150	71
RB	100	150	71
Wolf	100	150	71

Note: The Length parameter controls how accurately the filter is applied. Larger values produce less ringing but require more processor time.

Step 5 FK Filter slope values

Survey Line	Minimum Slope (ms/trace)	Maximum Slope (ms/trace	Maximum Frequency	Tapering power in FK Space
W	0	0.3	2000	0.3
V	0	0.4	2000	0.4
VB	0	0.4	2000	0.4
R	0	0.6	2000	0.6
RB	0	0.4	2000	0.4
Wolf	0	0.3	2000	0.3

Step 6 shot-gathered traces killed

Seismic Line – W				
Shot-Gather	First Trace Killed	Last Trace Killed	First Trace Killed	Last Trace Killed
3	1	3	21	24
4	1	3	21	24
5	1	3	21	24
6	1	3	21	24
7	1	3	21	24
8	1	3	21	24
9	1	3	21	24
10	1	3	21	24
11	1	3	21	24
12	1	3	21	24
13	1	3	21	24
14	1	3	21	24
15	1	3	21	24
16	1	3	21	24
17	1	3	21	24
18	1	3	21	24
19	1	5	21	24
20	1	7	21	24
21	1	9	20	24
22	1	9	20	24
23	1	11	20	24
24	1	11	20	24
25	1	13	20	24
26	1	13	20	24
27	1	14	20	24
28	1	15	20	24
29	1	16	20	24
30	1	17	20	24

Step 6 shot-gathered traces killed

Seismic Line - V				
Shot-Gather	First Trace Killed	Last Trace Killed	First Trace Killed	Last Trace Killed
1	1	3	12	14
2	1	3	12	14
3	1	3	12	14
4	1	3	12	14
5	1	3	12	14
6	1	3	12	14
7	1	3	12	14
8	1	3	12	14
9	1	3	12	14
10	1	3	12	14
11	1	3	12	14
12	1	3	12	14
13	1	3	12	14
14	1	3	12	14
15	1	3	12	14
16	1	3	12	14
37	1	3	9	12
38	1	3	9	12
39	1	3	9	12
40	1	3	9	12
41	1	3	9	12
42	1	3	9	12
43	1	3	9	12
44	1	3	9	12
45	1	3	9	12
46	1	3	9	12
47	1	3	9	12
48	1	3	9	12
61	1	3	1	4
62	1	3	1	5
63	1	3	1	6
63	1	3	1	7
64	1	3	1	8
65	1	3	1	9
66	1	3	1	10
67	1	3	1	11
68	1	3	1	12
69	1	3	1	13
70	1	3	1	14
71	1	3	1	15
72	1	3	1	16

Step 6 shot-gathered traces killed

Seismic Line - VB				
Shot-Gather	First Trace Killed	Last Trace Killed	First Trace Killed	Last Trace Killed
1	1	3	22	24
2	1	3	22	24
3	1	3	22	24
4	1	3	22	24
5	1	3	22	24
6	1	3	22	24
7	1	3	22	24
8	1	3	22	24
9	1	3	22	24
10	1	3	22	24
11	1	3	22	24
12	1	3	22	24
13	1	4	22	24
14	1	5	22	24
15	1	6	22	24
16	1	7	22	24
17	1	8	22	24
18	1	9	22	24
19	1	10	22	24
20	1	11	22	24
21	1	12	22	24

Step 6 shot-gathered traces killed

Seismic Line – R				
Shot-Gather	First Trace Killed	Last Trace Killed	First Trace Killed	Last Trace Killed
1	1	3	23	24
2	1	3	23	24
3	1	3	23	24
4	1	3	23	24
5	1	3	23	24
6	1	3	23	24
7	1	3	23	24
8	1	3	23	24
9	1	3	23	24
10	1	3	23	24
11	1	3	23	24
12	1	3	23	24
13	1	3	23	24
14	1	3	23	24
15	1	3	23	24
16	1	3	23	24
17	1	3	23	24
18	1	3	23	24
19	1	3	23	24
20	1	3	23	24
21	1	3	23	24
22	1	3	23	24
23	1	3	23	24
24	1	3	23	24
25	1	3	23	24
26	1	3	23	24
27	1	3	23	24
28	1	3	23	24
29	1	3	23	24
30	1	3	23	24
31	1	3	23	24
32	1	4	23	24
33	1	4	23	24
34	1	4	23	24
35	1	4	23	24
36	1	4	23	24
37	1	4	23	24
38	1	5	23	24
39	1	6	23	24
40	1	7	23	24
41	1	8	23	24
42	1	9	23	24
43	1	10	23	24
44	1	11	23	24
45	1	12	23	24
46	1	13	23	24
47	1	14	23	24
48	1	15	23	24

Step 6 shot-gathered traces killed

Seismic Line - RB								
Shot-Gather	First Trace Killed	Last Trace Killed	First Trace Killed	Last Trace Killed	First Trace Killed	Last Trace Killed	First Trace Killed	Last Trace Killed
1	1	5	12	16	23	24	-	-
2	1	5	12	16	23	24	-	-
3	1	5	12	16	23	24	-	-
4	1	5	12	16	23	24	-	-
5	1	5	12	16	23	24	-	-
6	1	5	12	16	23	24	-	-
7	1	5	12	16	23	24	-	-
8	1	5	12	16	23	24	-	-
9	1	5	12	16	23	24	-	-
10	1	5	9	10	12	16	23	24
11	1	5	12	16	23	24	-	-
12	1	5	12	16	23	24	-	-
13	1	8	12	16	23	24	-	-
14	1	7	12	16	23	24	-	-
15	1	8	12	16	23	24	-	-
16	1	9	12	16	23	24	-	-
17	1	16	23	24	-	-	-	-
18	1	16	23	24	-	-	-	-
19	1	16	23	24	-	-	-	-
20	1	16	23	24	-	-	-	-
21	1	16	23	24	-	-	-	-
22	1	16	23	24	-	-	-	-
23	1	16	23	24	-	-	-	-
24	1	17	23	24	-	-	-	-

Step 6 shot-gathered traces killed

Seismic Line - Wolf				
Shot-Gather	First Trace Killed	Last Trace Killed	First Trace Killed	Last Trace Killed
2	24	24	-	-
3	23	23	-	-
4	22	22	-	-
5	21	21	-	-
6	20	20	-	-
7	19	19	-	-
8	18	18	-	-
9	17	17	-	-
10	16	16	-	-
11	15	15	-	-
12	14	14	-	-
13	13	13	-	-
14	12	12	-	-
15	11	11	-	-
16	10	10	-	-
17	9	9	-	-
18	8	8	-	-
19	7	7	-	-
20	6	6	-	-
21	5	5	-	-
22	4	4	-	-
23	3	3	-	-
24	2	2	-	-
25	1	1	-	-
27	24	24	-	-
57	24	24	-	-
58	23	23	-	-
59	22	22	-	-
60	21	21	-	-
61	20	20	-	-
62	19	19	22	22
63	18	18	21	21
64	17	17	20	20
65	16	16	19	19
66	15	15	18	18
67	14	14	17	17
68	13	13	16	16
69	12	12	15	15
70	11	11	14	14
71	10	10	13	13
72	12	12	-	-
73	11	11	-	-
74	10	10	-	-
75	9	9	-	-
76	8	8	-	-

Step 8 CDP-gathered traces killed

Seismic Line - W		
CDP-Sorted Gather	First Trace Killed	Last Trace Killed
23	1	1
24	1	2
25	1	3
26	1	4
27	1	5
28	1	3
29	1	4
30	1	5
31	1	6
39	14	14
40	14	15
41	14	16
42	15	17
43	15	16
44	17	19
45	16	18
46	17	19
47	17	20
48	17	18
49	15	17
50	14	18
51	13	18
52	12	15
53	11	14
54	11	13
55	10	13
56	10	12
57	10	11
58	10	11
59	9	11
60	8	10
61	7	10
62	6	9
63	6	9
64	6	8
65	6	8
66	6	7
67	1	5
68	1	4
69	1	3
70	1	2
71	1	1

Step 8 CDP-gathered traces killed

Seismic Line - V						
CDP-Sorted Gather	First Trace Killed	Last Trace Killed	First Trace Killed	Last Trace Killed	First Trace Killed	Last Trace Killed
27	1	1	-	-	-	-
28	1	2	-	-	-	-
29	1	3	-	-	-	-
30	1	4	-	-	-	-
32	1	3	-	-	-	-
33	1	4	-	-	-	-
34	1	5	-	-	-	-
38	9	9	-	-	-	-
39	10	10	-	-	-	-
40	11	11	-	-	-	-
41	12	12	-	-	-	-
42	13	13	-	-	-	-
43	13	14	-	-	-	-
44	14	15	-	-	-	-
45	15	16	-	-	-	-
46	16	17	-	-	-	-
47	16	18	-	-	-	-
48	17	19	-	-	-	-
49	17	20	-	-	-	-
50	20	21	-	-	-	-
51	20	21	-	-	-	-
52	19	21	-	-	-	-
53	18	20	-	-	-	-
54	18	20	-	-	-	-
55	17	19	-	-	-	-
56	17	19	-	-	-	-
57	16	18	-	-	-	-
58	16	18	-	-	-	-
59	15	17	-	-	-	-
60	15	17	-	-	-	-
61	14	16	-	-	-	-
62	13	15	-	-	-	-
63	12	14	-	-	-	-
64	11	13	-	-	-	-
65	10	12	-	-	-	-
66	9	11	-	-	-	-
67	9	10	-	-	-	-
68	8	9	-	-	-	-
69	8	8	-	-	-	-
70	7	7	-	-	-	-
71	6	6	-	-	-	-
72	5	5	-	-	-	-
73	5	5	-	-	-	-
74	6	6	-	-	-	-
75	6	6	-	-	-	-
76	7	7	-	-	-	-
77	7	7	-	-	-	-
78	8	8	-	-	-	-
79	8	8	-	-	-	-
80	8	9	-	-	-	-
81	7	8	-	-	-	-

Seismic Line - V						
CDP-Sorted Gather	CDP-Sorted Gather	CDP-Sorted Gather	CDP-Sorted Gather	CDP-Sorted Gather	CDP-Sorted Gather	CDP-Sorted Gather
82	7	8	-	-	-	-
83	7	8	-	-	-	-
84	8	8	-	-	-	-
85	8	8	-	-	-	-
86	8	8	-	-	-	-
87	8	8	-	-	-	-
88	8	8	-	-	-	-
89	9	9	-	-	-	-
90	9	9	-	-	-	-
91	9	9	-	-	-	-
92	9	9	-	-	-	-
93	9	9	12	13	-	-
94	8	8	12	13	-	-
95	7	7	11	13	-	-
96	6	6	11	13	-	-
97	4	4	11	13	-	-
98	11	13	-	-	-	-
99	10	11	-	-	-	-
100	12	14	-	-	-	-
101	11	12	-	-	-	-
102	12	12	-	-	-	-
103	12	12	-	-	-	-
104	12	12	-	-	-	-
105	8	8	-	-	-	-
106	9	9	-	-	-	-
107	10	10	-	-	-	-
108	11	11	-	-	-	-
109	12	12	-	-	-	-
110	11	11	-	-	-	-
111	9	10	-	-	-	-
112	8	9	-	-	-	-
113	8	9	-	-	-	-
114	7	9	-	-	-	-
115	7	9	-	-	-	-
116	6	6	8	9	-	-
117	5	5	8	9	-	-
118	9	9	-	-	-	-
119	8	9	-	-	-	-
120	7	9	-	-	-	-
121	6	9	-	-	-	-
122	1	1	7	10	-	-
123	1	1	7	11	-	-
124	1	1	8	12	-	-
125	1	1	10	13	-	-
126	1	1	10	13	-	-
127	1	1	11	15	-	-
128	1	1	12	16	-	-
129	1	1	14	18	-	-
130	1	1	14	18	-	-
131	14	20	-	-	-	-
132	14	20	-	-	-	-
133	12	19	-	-	-	-

Seismic Line – V						
CDP-Sorted Gather	CDP-Sorted Gather	CDP-Sorted Gather	CDP-Sorted Gather	CDP-Sorted Gather	CDP-Sorted Gather	CDP-Sorted Gather
134	12	19	-	-	-	-
135	9	16	-	-	-	-
136	10	17	-	-	-	-
137	11	15	-	-	-	-
138	10	14	-	-	-	-
139	9	13	-	-	-	-
140	9	13	-	-	-	-
141	4	4	10	12	-	-
142	4	4	8	8	10	12
143	7	7	9	11	-	-
144	8	11	-	-	-	-
145	7	10	-	-	-	-
146	6	10	-	-	-	-
147	6	9	-	-	-	-
148	4	8	-	-	-	-
149	4	7	-	-	-	-
150	1	5	-	-	-	-
151	1	4	-	-	-	-
152	1	3	-	-	-	-
153	1	2	-	-	-	-
154	1	1	-	-	-	-

Step 8 CDP-gathered traces killed

Seismic Line - VB		
CDP-Sorted Gather	First Trace Killed	Last Trace Killed
13	1	1
14	1	2
15	1	3
16	1	4
17	1	5
23	8	8
24	9	9
25	9	10
26	11	11
27	11	12
28	11	13
29	12	15
30	13	15
31	12	17
32	15	17
33	13	18
34	12	17
35	14	18
36	13	17
37	12	16
38	13	15
39	12	15
40	12	13
41	12	13
42	12	13
43	11	13
44	10	12
45	10	11
46	9	10
47	8	9
48	4	8
49	4	7
50	1	5
51	1	4
52	1	3
53	1	2
54	1	1

Step 8 CDP-gathered traces killed

Seismic Line - R				
CDP-Sorted Gather	First Trace Killed	Last Trace Killed	First Trace Killed	Last Trace Killed
12	1	1	-	-
13	1	2	-	-
14	1	3	-	-
15	1	4	-	-
16	1	5	-	-
46	9	9	-	-
47	9	9	-	-
48	9	10	-	-
49	9	11	-	-
50	8	12	-	-
51	8	12	-	-
52	8	12	-	-
53	8	12	-	-
54	8	12	-	-
55	8	12	-	-
56	8	12	-	-
57	8	12	-	-
58	8	12	-	-
59	8	12	-	-
60	9	11	-	-
61	9	10	-	-
62	8	9	-	-
63	8	9	-	-
64	8	9	-	-
65	8	9	-	-
66	9	9	-	-
67	9	9	-	-
68	9	9	-	-
69	9	9	-	-
70	8	8	-	-
71	7	8	-	-
72	7	9	-	-
73	8	10	-	-
74	8	11	-	-
75	11	12	-	-
76	11	13	-	-
77	11	14	-	-
78	12	16	-	-
79	12	16	-	-
80	12	18	-	-
81	11	18	-	-
82	12	20	-	-
83	12	20	-	-
84	12	20	-	-
85	11	18	-	-
86	12	17	-	-
87	10	14	-	-
88	10	13	-	-
89	12	13	-	-

Seismic Line R				
CDP-Sorted Gather	CDP-Sorted Gather	CDP-Sorted Gather	CDP-Sorted Gather	CDP-Sorted Gather
90	11	14	-	-
91	11	12	-	-
92	10	12	-	-
93	9	11	-	-
94	8	8	-	-
95	9	10	-	-
96	9	10	-	-
97	8	9	-	-
98	7	9	10	11
99	6	8	-	-
100	6	7	-	-
101	1	5	-	-
102	1	4	-	-
103	1	3	-	-
104	1	2	-	-
105	1	1	-	-

Step 8 CDP-gathered traces killed

Seismic Line - RB		
CDP-Sorted Gather	First Trace Killed	Last Trace Killed
13	1	1
14	1	2
15	1	3
16	1	4
17	1	5
18	1	1
19	1	2
20	1	3
21	1	4
22	1	5
23	5	6
24	7	7
25	7	8
26	7	9
27	8	10
28	8	11
29	7	12
30	8	13
31	9	12
32	10	13
33	11	17
34	13	17
35	14	19
36	16	18
37	16	18
38	8	15
39	7	8
40	7	8
41	7	8
42	6	8
43	7	8
44	6	8
45	6	8
46	6	8
47	6	8
48	6	8
49	6	8
50	3	8
51	3	8
52	3	7
53	1	5
54	1	4
55	1	3
56	1	2
57	1	1

Appendix B: Seismic Reflection Geometry

Seismic geometry survey legend
Star: Source
Circle: Geophone

W Line:

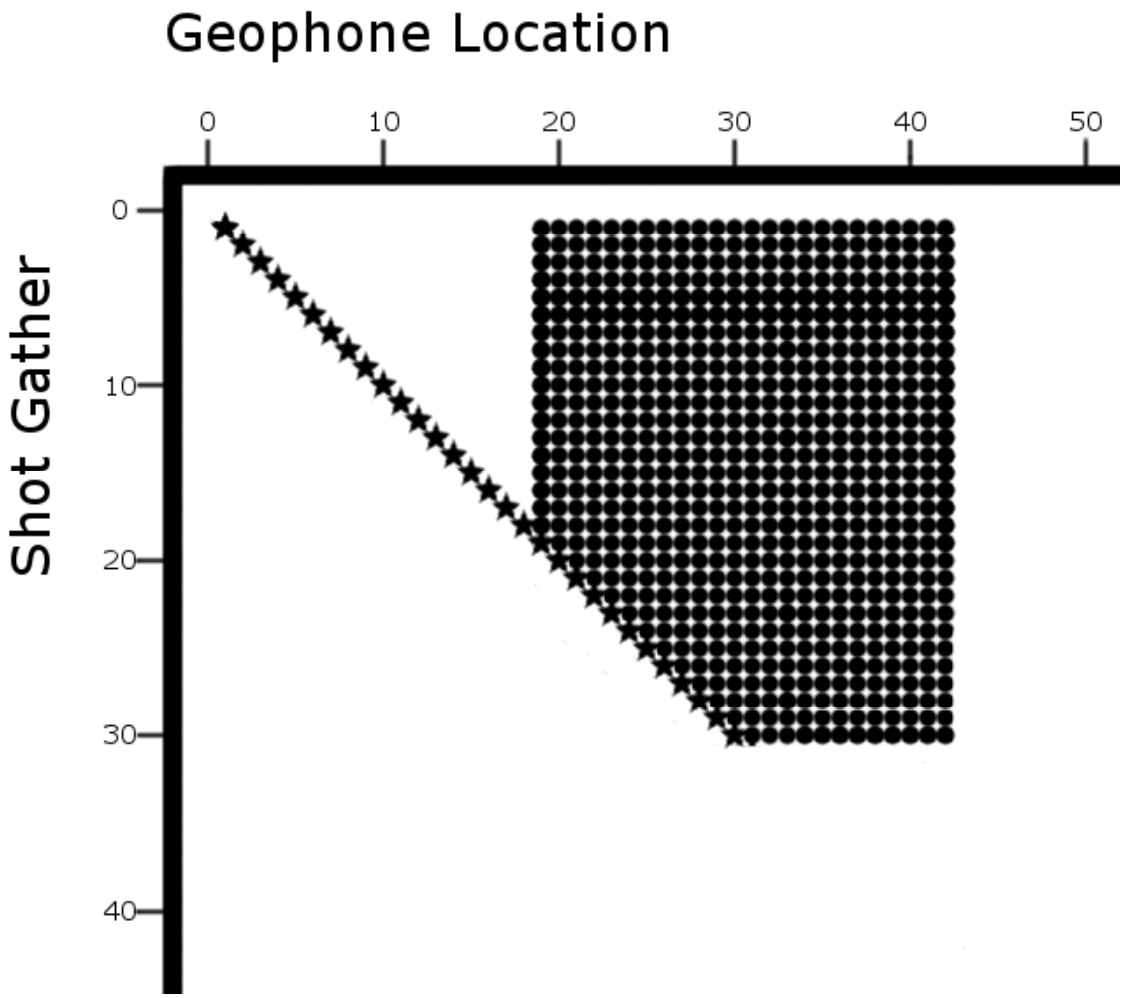

V Line:

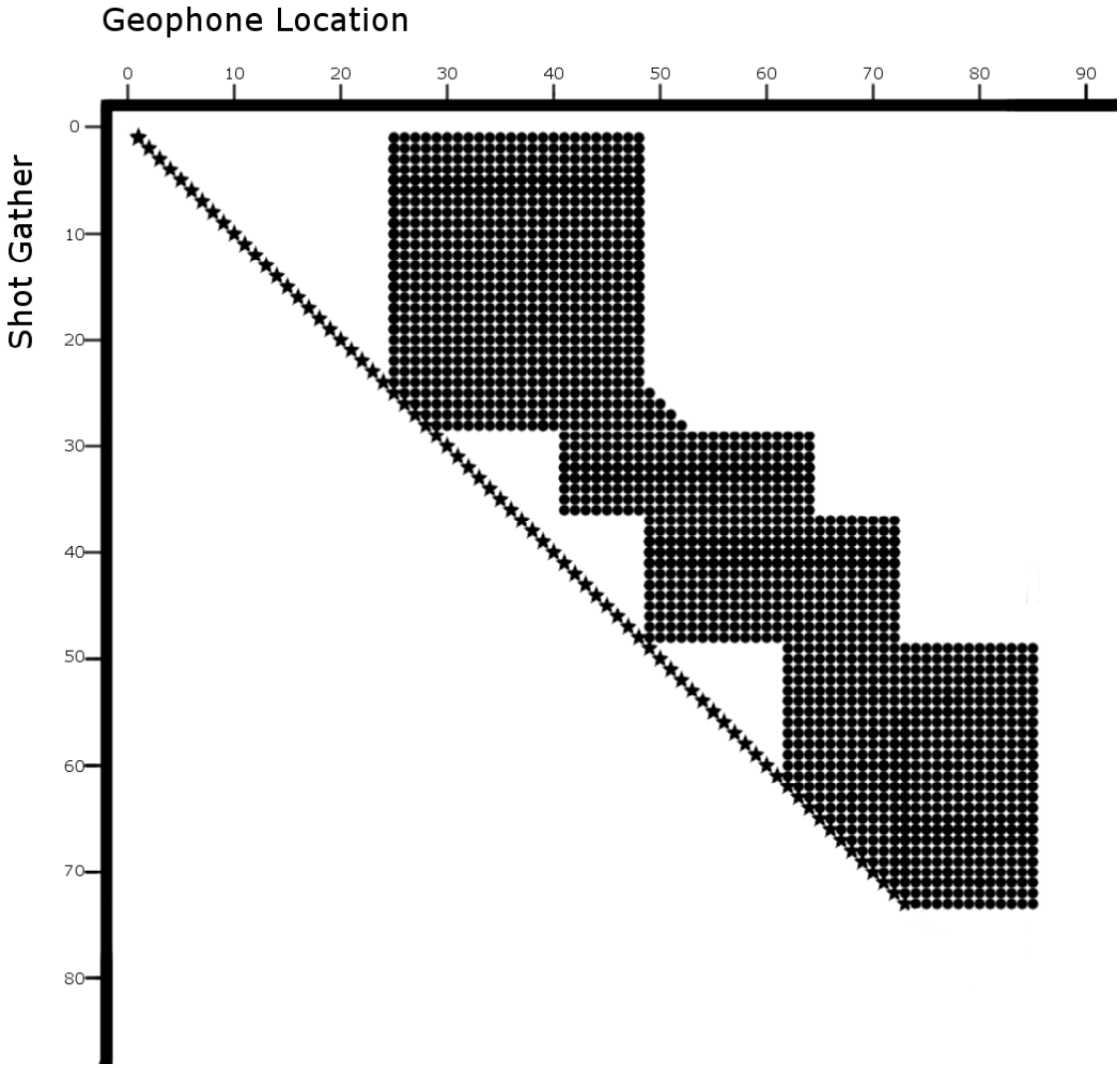
Geophone Location
0
10
20
30
40
50
60
70
80
90
Shot Gather
0
10
20
30
40
50
60
70
80

V_A Line:

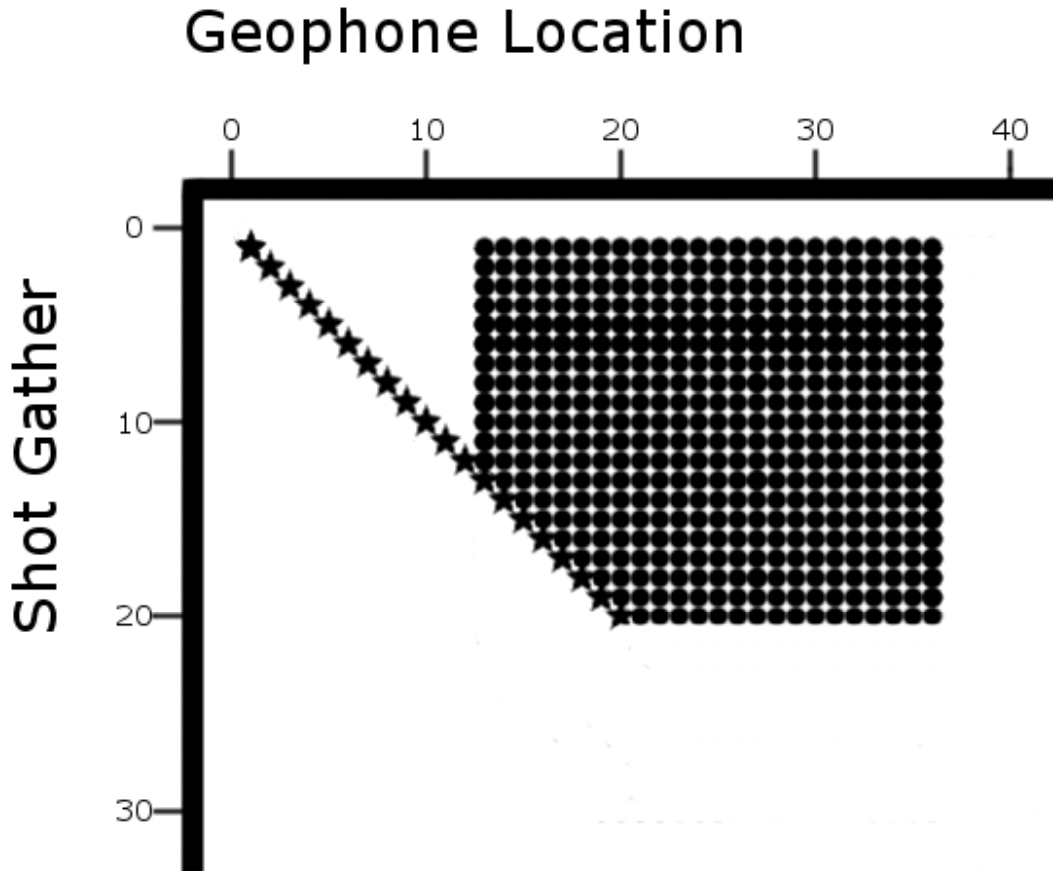

R Line:

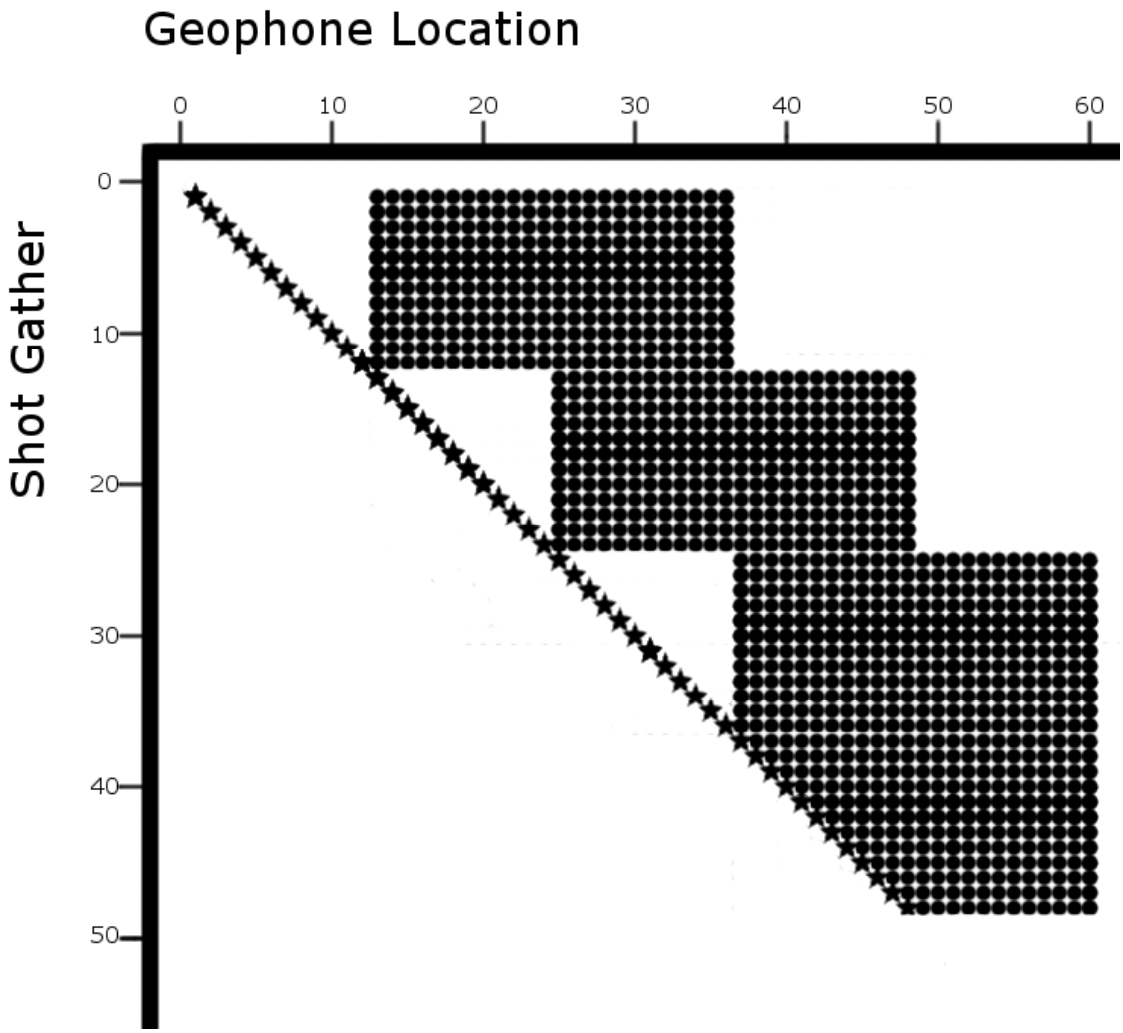
Geophone Location
0
10
20
30
40
50
60
Shot Gather
0
10
20
30
40
50

R_A Line:

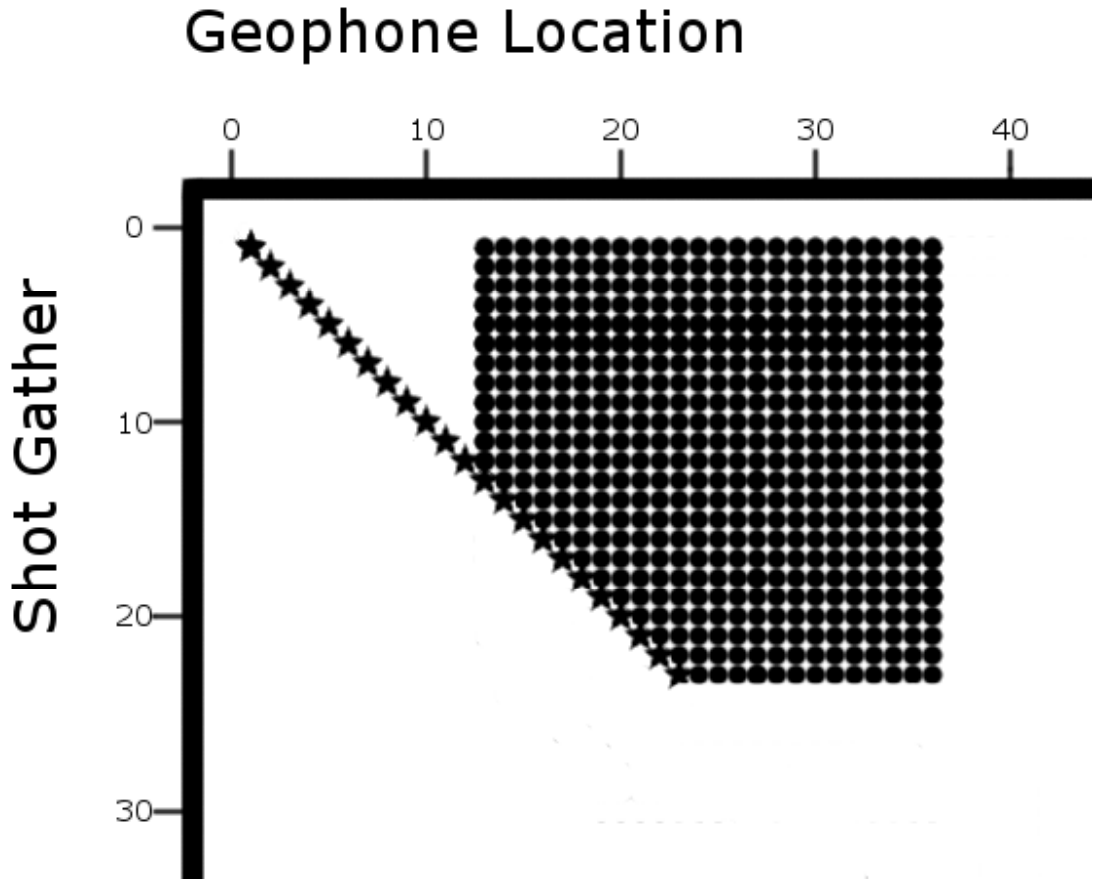

References:

Al-Shukri, H.J. and Mitchell, B.J., 1988, Reduced seismic velocities in the source zone of the New Madrid Seismic Zone; Bulletin of the Seismological Society of America, v. 78, n. 4, p. 1491-1509.

Al-Shukri, H.J. and Mitchell, B.J., 1990, Three dimensional attenuation structure in and around the New Madrid Seismic Zone; Bulletin of the Seismological Society of America, v. 80, n. 3, p. 615-632.

Austin, W.J., and Aslan, A., 2001, Alluvial pedogenesis in Pleistocene and Holocene Mississippi River deposits: Effects of relative sea-level change; GSA Bulletin, v. 113, n. 11, p. 1456-1466.

Austin, W.J., Burns, S.F., Miller, B.J., Saucier, R.T., and Snead, J.I., 1991, Quaternary geology of the lower Mississippi Valley; Quaternary Nonglacial Geology: Conterminous U.S., Geological Society of America, Boulder, CO, p. 547-582.

Baldwin, J.N., Harris, J.B., Van Arsdale, R.B., Gilver, R., Kelson, K.I., Sexton, J.L., and Lake, M., 2005, Constraints on the Location of the Late Quaternary Reelfoot Fault and New Madrid North Faults in the Northern New Madrid Seismic Zone, Central United States; Seismological Research Letters, v. 76, n. 6, p. 772-789.

Beck, A.E., 1981, Physical Principles of Exploration Methods; New York, Halsted Press, 234 p.

Braile, L.W., Hinze, W J. and Keller, G.R., 1997, New Madrid seismicity, gravity anomalies, and interpreted ancient rift structures; Seismological Research Letters, v. 68, p. 599-610.

Brocher, T.M., Nokleberg, W.J., Christensen, N.I., Lutter, W.J., Geist, E.L. and Fisher, M.A., 1991, Seismic reflection/refraction mapping of faulting and regional dips in the Eastern Alaska Range; Journal of Geophysical Research, v. 96, p. 10233-10249

Castilla, R.A. and Audemard, F.A., 2007, Sand blows as a potential tool for magnitude estimation of pre-instrumental earthquakes; Journal of Seismology, v. 11, p. 473-487

Chase Billeaudeau, http://en.wikipedia.org/wiki/User:ChaseBilleaudeau/sandbox, accessed 8/4/2013, updated 12/24/2012.

Claerbout, J.F., 1985, Fundamentals of Geophysical Data Processing; California, Blackwell Scientific Publishing, 274 p.

Cong, L., Mejia, J., and Mitchell, B.J., 2000, Attenuation dispersion of p waves near the New Madrid Seismic Zone; Bulletin of the Seismological Society of America, v. 90, n. 3, p. 679-689.

Cox, R.T. and Van Arsdale, R.B, 2002, The Mississippi embayment, North America: A first order continental structure generated by the Cretaceous superplume mantle event; Journal of Geodynamics, v. 34, p. 163-176.

Csontos, R. and Van Arsdale, R., 2008, New Madrid Seismic Zone fault geometry; Geological Society of America, v. 4, p. 802-813.

Csontos, R.., Van Arsdale, R., Cox, R., and Waldron, B., 2008, Reelfoot rift and its impact on Quaternary deformation in the central Mississippi River valley; Geological Society of America, n. 4, v. 145-158.

Davis, G.H. and Reynolds, S.J., 1996, Structural Geology: of Rocks and Regions; John Wiley and Sons, 775 p.

Dunn, M., Horton, S., DeShon, H., and Powell, C., 2010, High-resolution earthquake relocation in the New Madrid Seismic Zone; Seismological Research Letters, v. 81, n. 2, p. 406-413.

Fuller, M.L., 1912, The New Madrid earthquake: U.S. Geological Survey Bulletin, v. 494, p. 1-120.

Gomberg, G. and Ellis, M., 1994, Topography and tectonics of the central New Madrid seismic zone: results of numerical experiments using a three-dimensional boundary element program; Journal of Geophysical Research, v. 99, p. 20299-20310.

Guccione, M.J., Marple, R., and Autin, W.J., 2005, Evidence for Holocene displacements on the Bootheel fault (lineament) in southeastern Missouri: Seismotectonic implications for the New Madrid region; Bulletin of the Geological Society of America, v. 117, p. 319-333.

Hackley, P.C., Warwick, P.D., Thomas, R.E., and Nichols, D.J., 2006, Review of lignite resources of Western Tennessee and the Jackson Purchase area, Western Kentucky; USGS Open File Report, Report # 2006-1078, 34 p.

Harden, J.W., and Taylor, E.M., 1983, A quantitative comparison of soil development in four climatic regions; Quaternary Research, v. 20, p. 342-359

Harding, T.P., 1985, Seismic Characteristics and Identification of Negative Flower Structures, Positive Flower Structures, and Positive Structural Inversion; AAPG Bulletin, v. 69, n. 4, p. 582-600.

Hardy, Basic Seismic Processing for Interpreters; www.xsgeo.com, accessed 4/21/2013, last updated 2008.

Harris, J.B., 2009, Hammer-impact SH-wave seismic reflection methods in neotectonic investigations: General observations and case histories from the Mississippi Embayment, U.S.A.; Journal of Earth Science, v. 20, n. 3, p. 513-525.

Herrmann, R.B. and Canas, J., 1978, Focal mechanism studies in the New Madrid seismic zone: Bulletin of the Seismological Society of America, v. 68, n. 4, p. 1095-1102.

Johnston, A.C. and Nava, S.J., 1995, Recurrence rates and probability estimates for the New Madrid seismic zone; Journal of Geophysical Research, v. 90, p. 6737-6753.

Johnston, A.C., 1996, Seismic moment assessment of stable continental earthquakes, Part III: 1811-1812 New Madris, 1886 Charleston, and 1755 Lisbon; Geophysical Journal International, v 126, p. 314-344.

Kearey, P. and Brooks, M., 1991, An Introduction to Geophysical Exploration, Second Edition; Oxford, Blackwell Scientific Publications, 254 p.

Kenner, S.J. and Segall, P., 2000, A mechanical model for intraplate earthquakes: Application to the New Madrid Seismic Zone; Science, v. 289, p. 2329-2332.

Liu, L. and Li, Y., 2001, Identification of liquefaction and deformation features using ground penetration radar in the New Madrid seismic zone, USA; Journal of Applied Geophysics, v. 47, i. 3-4, p. 199-215.

Liu, L. and Zoback, M.D., 1999, Lithospheric strength and interpolate seismicity in the New Madrid seismic zone; Tectonics, v. 16, no. 4, p. 585-595.

Liu, Z., Wuenscher, M.E., and Herrmann, R.B., 1994, Attenuation of Body Waves in the central New Madrid Seismic Zone; Bulletin of the Seismological Society of America, v. 84, n. 4, p. 1112-1122.

McCaplin, J.P., 1996, Paleoseismology; San Diego, Academic Press, 588 p.

Mueller, K., Champion, J., Guccione, M. and Kelson, K., 1999, Fault Slip Rates in the Modern New Madrid Seismic Zone; Science, v. 286, p. 1135-1138.

Mueller, K., Hough, S.E. and Billham, R., 2004, Madrid earthquakes with recent instrumental recorded aftershock; Nature, v 429, p. 284-288.

Mueller, K. and Pujol, J, 2001, Three-Dimensional Geometry of the Reelfoot Blind Thrust: Implications for Moment Release and Earthquake Magnitude in the New Madrid

Seismic Zone; Bulletin of the Seismological Society of America, v. 91, n. 6, p. 1563-1573.

Nelson, K. D. and Zhang, J., 1991, A COCORP deep reflection profile across the buried Reelfoot Rift, south-central United States; Tectnophysics, v. 197, p. 271-293.

Nelson, J.W., 1998, Bedrock geology of the Paducah 1°x2° CUSMAP quadrangle, Illinois, Indiana, Kentucky, and Missouri; U.S. Geological Survey Bulletin, n. 2150-B, v. 36.

Obermeier, S.F., 1989, The New Madrid Earthquakes: an engineering-geologic interpretation of relict liquefaction features; U.S. Geological Survey Professional Paper 1336-B, 114 p.

Obermeier, S.F., Martin, J.R., Frankel, A.D., Youd, T.L. Munson, P.J., Munson, C.A. and Pond, E.C., 1993, Liquefaction evidence for one or more strong Holocene earthquakes in the Wabash Valley of Southern Indiana and Illinois, with a preliminary estimate of magnitude; USGS Professional Paper 1536.

Park, C.B., Miller, R.D., and Ivanov, J., 2002, Filtering Surface Waves; Proceedings of the SAGEEP 2002, Las Vegas, Nevada.

Parrish, S. and Van Arsdale, R., 2004, Faulting along the southeastern margin of the Reelfoot Rift in northwestern Tennessee revealed in deep seismic-reflection profiles; Seismological Research Letters, v. 75 p. 784-793.

Russ, D.P., 1982, Style and significance of surface deformation in the vicinity of New Madrid, Missouri; in Investigations of the New Madrid, Missouri, Earthquake Region, US Geological Survey Professional Papers, v. 1236, p. 95-114.

Saucier, R.T., 1989, Evidence for episodic sand-blow activity during the 1811-1812 New Madrid (Missouri) earthquake series: Geology, v. 17, p. 103-106.

Saucier, R.T., 1994, Geomorphic and Quaternary geologic history of the lower Mississippi Valley; U.S. Corps of Engineers Waterways Experiment Station, v. 364.

Sexton, J.L. and Jones, P.B., 1988, Mini-sosie high-resolution reflection survey of the Cottonwood Grove Fault in northwestern Tennessee; Bulletin of the Seismological Society of America, v. 78, n. 2, p. 838-854.

Schweig, E.S. and Ellis, M.A., 1994, Reconciling short recurrence interval with minor deformation in the New Madrid Seismic Zone; Science, v. 264, p. 1308-1311.

Shaw, J.H., Hook, S.C., and Sitohang, E.P., 1997, Extensional Fault-Bend Folding and Synrift Deposition: An Example from the Central Sumatra Basin, Indonesia; AAPG Bulletin, v. 81, n. 3, p. 367-379.

Shumway, A.M., 2008, Focal mechanisms in the northeast New Madrid Seismic Zone; Seismological Research Letters, v. 79, n. 3, p. 469-477.

Soil Survey Staff, 2010, Keys to Soil Taxonomy, 11th ed; USDA-Natural Resources Conservation Service, Washington, DC.

Steeples, D.W., and Miller, R.D., 1998, Avoiding pitfalls in shallow seismic reflection surveys; Geophysics, v. 63, n. 4, p. 1213-1224.

Tavakoli, B., Pezeshk, S., and Cox, R.T., 2010, Seismicity of the New Madrid Seismic Zone derived from a deep-seated strike-slip fault; Bulletin of the Seismological Society of America, v. 100, n. 4, p. 1646-1658.

Tuttle, M.P., 2001, The use of liquefaction features in paleoseismology: Lessons learned in the New Madrid seismic zone, central United States; Journal of Seismology, v. 5, p. 361-380.

Tuttle, M.P. and Barstow, N., 1996, Liquefaction-related ground failure: A case study in the New Madrid seismic zone, Central United States; Bulletin of the Seismological Society of America, v. 86, n. 3, p. 636-645.

Tuttle, M.P. and Schweig, E.S., 1995, Archeological and pedological evidence for large prehistoric earthquakes in the New Madrid seismic zone, central United States; Geology, v. 23, no. 3, p. 253-256.

Tuttle, M.P., Schweig, E., III, Campbell, J., Thomas, P. M., Sims, J.D. and Lafferty, R.H., III, 2005, Evidence for New Madrid earthquakes in A.D. 300 and 2350 B.C., Seismological Research Letters, v. 76, n. 4, p. 489-501.

Tuttle, M.P., Schweig, E.S., Sims, J.D., Lafferty, R.H., Wolf, L.W. and Haynes, M.L., 2002, The Earthquake Potential of the New Madrid Seismic Zone; Bulletin of the Seismological Society of America, v. 92, no. 6, p. 2080-2089.

Tuttle, M.P., Schweid, E.S., Campbell, J, Thomas, P.M., Sims, J.D., and Lafferty, R.H., 2005, Evidence for New Madrid Earthquakes in A.D. 300 and 2350 B.C; Seismological Research Letters, v. 76, n. 4, p. 489-501.

Tuttle, M.P., Sims, J.D., Dyer-Williams, K., Lafferty, R.H., and Schweig, E.S., 2000, Dating of Liquefaction Features in the New Madrid Seismic Zone; U.S. Nuclear Regulatory Commission, 91 p.

US Geological Survey, 2011, Report of the Independent Expert Panel on New Madrid Seismic Zone Earthquake Hazard; NMSZ Expert Panel Report to the NEPEC, 26 p.

US Geological Survey Earthquakes, Tennessee Earthquake Information, http://earthquake.usgs.gov/regional/states/?region=tennessee, accessed 7/15/09, updated 6/26/09

Van Arsdale, R.B., 2000, Displacement history and slip rate on the Reelfoot fault of the New Madrid seismic zone: Engineering Geology, v. 55, p. 219-226.

Van Arsdale, R.B., Williams, R.A., Schweig, E.S., Shedlock, E.S., Odum, J.K., and King, K.W., 1995, The origin of Crowley's Ridge, northeastern Arkansas: erosional remnant or tectonic uplift?; Seismological Society of America Bulletin, v. 85, p. 963-985.

Van Arsdale, R.B., Purser, J., Stephenson, W., and Odum, J., 1998, Faulting along the southern margin of Reelfoot Lake, Tennessee; Seismology Society Annual Bulletin, v. 88, p. 131-139.

Van Arsdale, R.B. and TenBrink, R.K., 2000, Late Cretaceous and Cenozoic geology of the New Madrid Seismic Zone; Bulletin of the Seismological Society of America, v. 90, p. 345–356.

Velasco, M., Van Arsdale, R., Waldron, B., Harris, J., and Cox, R., 2005, Quaternary Faulting beneath Memphis, TN; Seismological Research Letters, v. 76, n. 5, p. 598-614.

Walker, R.G., and James, N.P., 1992, Facies Models: Response to Sea Level Change; Canada, Geological Association of Canada, 454 p.

Woolery, E.W., Street, R.L., Wang, Z., Harris, J.B., and McIntyre, J., 1999, Neotectonic Structure in the Central New Madrid Seismic Zone: Evidence from Multimode Seismic Reflection Data; Seismological Research Letters, v. 70, n. 5, p. 554-576.

Acknowledgements

Dr Martitia Tuttle

US Geological Survey

Boston College Department of Earth and Environmental Sciences

Natasha McCallister, US Geological Survey

Michael Towle, Center for Earthquake Research and Investigation

Dr Nathan Moran, University of Memphis

Douglas Jorgensen